INSTITUTE OF PHYSICS PUBLISHING JOURNAL OF OPTICS A: PURE AND APPLIED OPTICS
J. Opt. A: Pure Appl. Opt. **3** (2001) S103–S120 PII: S1464-4258(01)27690-9

Photonic bandgap materials: towards an all-optical micro-transistor

Sajeev John and Marian Florescu[1]

Department of Physics, University of Toronto, Toronto, Ontario, Canada M5S 1A7

E-mail: marian@physics.utoronto.ca

Received 7 August 2001, in final form 21 September 2001
Published 26 October 2001
Online at stacks.iop.org/JOptA/3/S103

Abstract
We describe all-optical transistor action in photonic bandgap (PBG) materials doped with active atoms and analyse the advantages of this system over other all-optical transistor proposals. In the presence of a PBG material, a coherent laser beam with the frequency slightly detuned from the resonant atomic transition frequency can drive a collection of two-level atoms to an almost totally inverted state, a phenomenon strictly forbidden in ordinary vacuum. By varying the laser field intensity in the neighbourhood of a threshold value, it is possible to drive the atomic system through a transition from states in which the atoms populate preferentially the ground level to almost totally inverted states. In this process, the atomic system switches from a passive medium (highly absorptive) to a active medium (highly amplifying). The large differential gain exhibited by the atomic medium is very robust with respect to nonradiative relaxation and dephasing mechanisms. The switching action in a PBG material is not associated with operation near a narrow cavity resonance with conventional trade-off between switching time and switching threshold intensity. Rather it is associated with an abrupt discontinuity in the engineered broad-band electromagnetic density of states of the PBG material. We demonstrate all-optical transistor action in PBG materials by analysing the absorption spectrum of a second probe laser beam and we show that the probe beam experiences a substantial differential gain by slight intensity modulations in the control laser field. Under certain conditions, the fluctuations in the number of totally inverted atoms that contribute to the amplification process are strongly diminished (the statistics of the excited atoms becomes sub-Poissonian), which, in turn, determines a very low-noise regime of amplification.

Keywords: All-optical transistor, all-optical switching, photonic bandgap materials, collective atomic switching, resonance flourescence

(Some figures in this article are in colour only in the electronic version)

1. Introduction: all-optical transistor action

The transmission of information as optical signals encoded on light waves travelling through optical fibres and optical networks is increasingly moving to shorter and shorter distance scales. In the near future, optical networking is poised to supersede conventional transmission over electric wires and electronic networks for computer-to-computer communications, chip-to-chip communications and even on-chip communications. The ever-increasing demand for faster and more reliable devices to process the optical signals offers new opportunities in developing all-optical signal processing systems (systems in which one optical signal controls another, thereby adding 'intelligence' to the optical networks). All-optical switches, two-state and many-state all-optical

[1] To whom correspondence should be addressed.

memories, all-optical limiters, all-optical discriminators and all-optical transistors [1] are only a few of the many devices proposed during the last two decades. In particular, it has been suggested that electronic transistors may one day be replaced by all-optical transistors, which will perform all the operations that their electronic counterparts do: amplification, switching, modulation and detection. The 'all-optical' label is commonly used to distinguish the devices that do not involve dissipative electronic transport [2] and require essentially no electrical communication of information. The all-optical transistor action was first observed in the context of optical bistability [1, 3] and consists in a strong differential gain regime, in which, for small variations in the input intensity, the output intensity has a very strong variation, $\mathrm{d}I_\mathrm{T}/\mathrm{d}I_\mathrm{I} > 1$ (I_T is the output intensity and I_I the input intensity). This analogue operation is for all-optical input what transistor action is for electrical inputs. The emerging competition between all-optical devices and their electronic counterparts brings with it significant practical challenges. The most important demand is related to the integration of the all-optical devices. In order to achieve an all-optical chip, the individual components should have length scales of the 10 micrometre order. In order to diminish the heating of the chip and the operating power, the holding power and the switching energy should be minimized. The switching time of the device should be below 1 ps (the fastest GaAs transistor has a switching time of about 20 ps). The large number of interconnections on an all-optical chip should be insensitive to environmental perturbation and should operate at room temperature.

1.1. Saturable absorbers and third-order nonlinear mechanisms

Saturable absorbers (e.g. Na vapour) and third-order nonlinearities (Kerr media) were among the earliest options for all-optical processing and switching. The system of choice is a Fabry–Perot cavity, filled with Na vapour or a Kerr medium with a cubic dielectric susceptibility $\chi^{(3)}$ [1, 3–5]. The basic principle of transistor action in nonlinear Fabry–Perot interferometers is that very small optically induced changes in the refractive index of the filling medium can be used to control the magnitude of the output optical signal. The nonlinear Fabry–Perot resonator consists of a pair of plane, partially reflecting mirrors surrounding a nonlinear medium (in the initial proposal, Na vapour [6]) whose index of refraction depends on the optical intensity within it. In resonance conditions, an integral number of half wavelengths of light would fit inside the cavity. Initially, the device is tuned slightly off resonance. With increasing input power, the intensity inside the resonator increases, thereby changing the index of refraction of the cavity, and pulling it towards the resonant condition. This in turn increases the intensity inside the cavity and, implicitly, gives yet further change in the index of refraction and so on. The positive feedback mechanism that combines the optical nonlinearity of the material with the external feedback from the resonance of the cavity can become very strong and provide a strong differential gain for relatively small changes in the input intensity. Optical transistor action is obtained by inducing a weak modulation in the input beam [3, 6] or by introducing a weak-magnitude second pump beam (see figure 1). By replacing the Na vapour with a medium with a very large $\chi^{(3)}$, the threshold switching intensity is dramatically reduced, while the differential gain is strongly enhanced. In [7], Miller and Smith were the first to obtain two-beam amplification and they have used a semiconductor crystal of InSb, 580 μm thick, with polished parallel faces held at 5 K in a helium cryostat as a nonlinear Fabry–Perot interferometer. The effective $\chi^{(3)}$ nonlinearity was of the order of 10^{-2} esu (this huge value was explained in terms of a combination between semiconductor bandgap effects and power broadening). The transistor action is obtained by adding to the input 'holding' incident beam (the control beam) a low-power chopped beam as a 'signal' and the 'optical bias' is increased until gain is observed. By improving the fabrication of the device, Tooley *et al* [8] increased the operating temperature to 77 K and decreased the holding power to 5 mW. The differential gain of their device could be as high as 10^4.

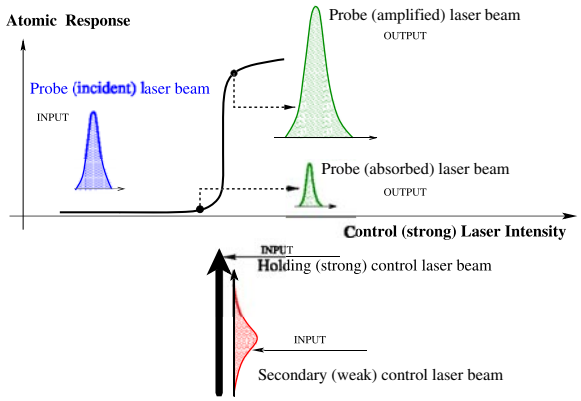

Figure 1. Schematic description of the transistor action [1]. The system response exhibits a strong variation at a well defined threshold value of the control laser field intensity. A second weak control laser field (whose magnitude is determined by the width of the threshold region between absorbing and amplifying states) is used to switch the device. An incident probe beam will be absorbed or amplified depending upon the magnitude of the total control laser field.

1.2. Other approaches

Another option for all-optical signal processing involves the nonlinear phase shift induced by the transfer of energy between the fundamental and the second-order harmonic waves (cascaded second-order nonlinearities) [9–11]. This requires lower power and takes advantage of the technological advances in noncentrosymmetric materials [12, 13]. Nonlinear interactions based on quadratic effects are usually coherent and allow both phase and amplitude modulation [14]. The nonlinear phase shift of the fundamental wave in a cascaded $\chi^{(2)}$ process arises from a chain process [15]. Transistor action in this approach is described in a simple picture in [16, 17]. A 3 cm long version of a waveguide second-harmonic converter in periodically domain-inverted $LiNbO_3$ [18] allows a 1 W infra-red pump wave to be controlled by a 1 μW injected second-harmonic signal.

Datskos and Rajic[2] have proposed an all-optical transistor based on photo-induced stress in semiconductors. The laser

[2] 14 February 2000, Oak Ridge National Laboratory, Media Release.

light from a diode laser (LED) is absorbed in a waveguide material. The absorption of light causes stress in the host material, which in turn strains the material and produces a small displacement of it. The primary micro-mechanical waveguide (source) feeds two other micro-mechanical waveguide channels (drains) and a control microstructure (gate). Switching is controlled by minor disruptions (waveguide deflections) of the evanescent field. This way, the device can redirect light coming from one end onto two or more channels and becomes actually equivalent to an electric switch or modulator used in conventional electronic transistors. Coriasso *et al* [19] reported all-optical switching and pulse-routing functionality of nonlinear multiple-quantum-well ridge waveguides equipped with a Bragg grating. In a similar system, single-wavelength all-optical transistor action in a GaAs/AlAs multiple-quantum-well hetero-nipi waveguide structure has also been shown in [20].

The major drawbacks of these proposals are related to their size (most of the devices cannot be scaled down to spatial extensions smaller than 300 μm), their switching times and their high power requirements. The switching time of the device is limited by cavity build-up time, cavity dynamical effects and nonlinear medium response time. For example, by operating very close to a very narrow cavity resonance, the switching threshold can be reduced, whereas cavity build-up time increases dramatically. Consequently the product of the switching threshold and switching time remains unacceptably large. Using materials with large optical nonlinearities also requires a compromise in the response time of the medium. Other physical limitations include the lack of scalability and integrability.

2. Low-threshold all-optical switching and transistor action near a photonic bandgap

Photonic bandgap (PBG) materials constitute a new class of dielectrics which carry the concept of moulding and controlling the flow of light to its most microscopic level. This is entailed in a fundamentally new optical principle, namely the localization of light [21, 22], and leads to the inhibition of spontaneous emission [23], the formation of the photon–atom bound states [24], very low-threshold nonlinear optical phenomena [25] and low-threshold collective atomic switching behaviour. Previous studies [26] suggest that a laser operating near a photonic band edge may possess unusual spectral and statistical properties, as well as a low input power threshold. In certain conditions, a doped photonic crystal exhibits low-threshold optical bistability in the atomic response to an applied laser field [27]. In the context of all-optical transistor action, the photonic band edge, which separates the PBG from the continuum of propagating electromagnetic modes, facilitates fundamental switching effects for resonant two-level systems that are forbidden in ordinary vacuum. In particular, the Einstein rate equations [28], when applied to a collection of two-level atoms coherently pumped near resonance in ordinary vacuum, forbid atomic population inversion in the steady-state limit. Such inversion often plays a key role in the laser light emission. As a consequence, it is customary to pump an active medium to a higher level, followed by incoherent relaxation to the (population-inverted) excited level that defines the lasing transition. This type of switching from the ground to the excited state involves incoherent processes and makes the conventional laser unsuitable as an ultra-fast optical switch or transistor. Moreover, the pumping threshold required to achieve inversion may be unsuitable for all-optical information processing. On the other hand, in a photonic crystal, a coherent laser beam with the frequency slightly detuned from the atomic transition frequency can drive a two-level atom to almost totally inverted atomic states [25, 29]. In this process, the atomic system switches from a passive medium (highly absorptive) to a gain medium (highly amplifying), as a function of the external driving field. The large differential gain exhibited by the atomic medium is very robust with respect to nonradiative relaxation and dephasing mechanisms [29] (associated with atomic collisions or scattering of phonons from the dielectric lattice on the atomic system [30]). This switching effect exhibits collective enhancement when there are many two-level atoms within a cubic wavelength inside the PBG material [25]. In this case, the ensemble of atoms sharply switches to a highly inverted state at a sharp threshold value of the applied laser pump intensity.

A doped PBG material may, in this sense, be used as an ultra-fast all-optical switch and an all-optical micro-transistor. Similar to other all-optical transistor proposals [1], the transition between the absorptive and the amplifying regime can be modulated with a weak second control laser field (in phase and in resonance with the main strong pump field). Unlike other proposals, such as the one described in section 1.1, the switching effect is not limited to the coupling of light to a narrow cavity resonance in which there is a conventional (inverse) relationship between the switching (cavity build-up) time and the switching intensity threshold. Instead, the PBG-based switching effect requires the coupling of light emitters to a broad-band electromagnetic density of modes in which there is a sharp (discontinuous) jump over a narrow frequency interval. The engineering of the defect structure within a three-dimensional PBG provides considerable latitude in the development of such a device heterostructure. As we show in section 5, a probe laser field of prescribed wavelength will experience a substantial differential gain by slight modulations in the weak control laser field. Under certain conditions, the fluctuations in the number of the excited atoms that contribute to the amplification process can be strongly diminished (the statistics of the excited atoms become sub-Poissonian [25]), which in turn determines a low-noise regime of amplification.

2.1. Optical mode density near a photonic bandgap

PBG materials typically consist of a two inter-penetrating dielectric components. The first is a connected high-dielectric-constant backbone, and the second is a connected low-dielectric-constant network. For example, a network of criss-crossing pores in a semiconductor of refractive index 3.5 [31], or a woodpile structure [32, 33] can provide bandgaps of 20% of the central frequency of the gap. A detailed review of recent advances in the fabrication of three-dimensional PBG materials is given in [34]. A fabrication method using photo-electrochemical etching pores has also been proposed in [35, 36]. A recent breakthrough using self-assembly methods [37–40], is a silicon-based inverse opal

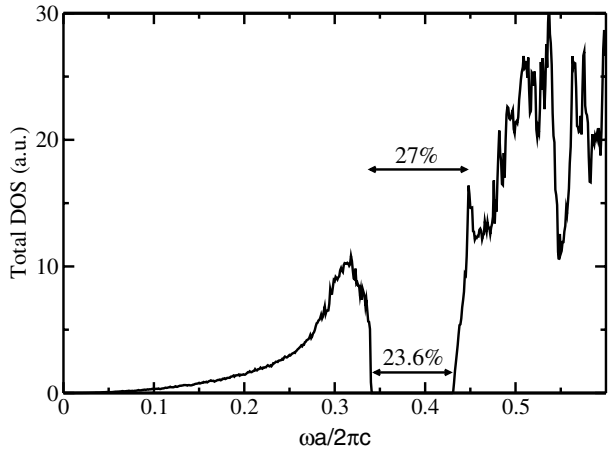

Figure 2. The total electromagnetic density of states for an optimized inverted square spiral structure [42]. Here ω is the frequency of the light, a is the lattice constant of the dielectric structure and c the speed of light.

three-dimensional photonic crystal with a 5% complete three-dimensional PBG centred near 1.5 μm [41]. Very recently [42] a blueprint for a three-dimensional PBG material amenable to large-scale micro-fabrication on the optical scale, based on glancing angle deposition methods, has been suggested. The proposed chiral crystal consists of square spiral posts on a tetragonal lattice, and for silicon posts in air background (direct structure) exhibits a full bandgap of 15% of the central frequency, while for the inverse structure (air posts in a silicon background) the bandgap can be as large as 24%. The photon density of states for this inverse square spiral is shown in figure 2.

In a real three-dimensional PBG material, the electromagnetic modes near the upper photonic band edge are concentrated in the air fraction of the composite material, and accordingly, this is referred to as the air band. Near the lower photonic band edge, the electromagnetic energy is concentrated in the high-dielectric backbone. Accordingly, this is referred to as the dielectric band. The active 'two-level atoms' in our model calculation can be embedded as quantum dots in the dielectric backbone or may be laser cooled and trapped into the void regions of the PBG material [43]. As can be seen from figure 2, if the two-level atomic resonance occurs near a photonic band edge, the density of electromagnetic modes available to the atomic transition varies very rapidly with frequency. Inside the gap this density vanishes, whereas just outside the gap the density may exceed that of ordinary vacuum. The ability of an external pump laser to switch spectral characteristics of the atomic system across the band edge (or near any other discontinuous density of states profile) leads to coherent all-optical switching and transistor action. In figure 3, we show an artist's view of an all-optical transistor based on a three-dimensional PBG. The heterostructure consists of a three-dimensional PBG template into which a sequence of III–V semiconductors has been infiltrated. The middle layer, which acts as a planar waveguide inside a three-dimensional PBG, is an active region (quantum dots) sandwiched between semiconductor cladding layers. The active region is assumed to experience a band edge type discontinuity within the larger three-dimensional PBG. The laser beam from above the structure constitutes the main

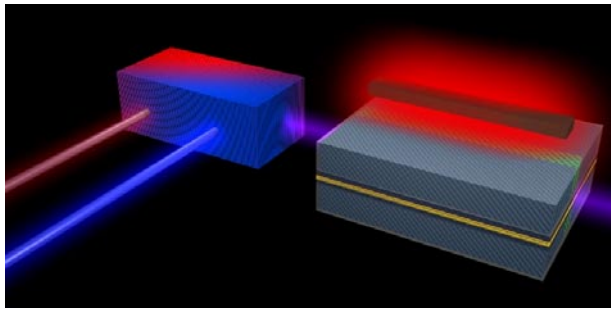

Figure 3. Possible device heterostructure for all-optical switching and transistor action. From the left, two low-intensity laser beams enter the heterostructure from optical fibres combined by a coupler. The heterostructure consists of a planar waveguide region, containing quantum dots, sandwiched by a three-dimensional PBG. From above, the heterostructure is illuminated by the main control (pump) laser field. On the right of the figure is the amplified signal field as it leaves the heterostructure.

control (pump) laser field, which drives the 'atomic' system embedded in the square spiral heterostructure. From the left, two low-intensity laser beams enter the heterostructure from optical fibres combined by a coupler, as shown on the left of the figure. One of them adds to the main pump beam with the role of switching the active medium between the absorptive and amplifying regimes. The second beam constitutes the signal field, which is amplified or absorbed (depending on the magnitude of the modulated component of the pump field) as it propagates through the active medium.

3. Single-atom switching in photonic bandgap materials

We begin by reviewing the conventional picture of atom–field interaction, in which a coherent laser field with an average incident energy density W and frequency ω, interacts with a collection of N independent two-level atoms in ordinary vacuum. In the most simplified picture, the dynamical and steady-state behaviour of the atomic system is governed by the Einstein rate equations, obtained under the assumption that the density of states characterizing the photonic reservoir is slowly varying with the frequency. The rate equation (based on Fermi's golden rule for absorption and emission) is

$$\frac{\mathrm{d}N_2}{\mathrm{d}t} = -(A + B_{\mathrm{ab}}\, W)N_2 + B_{\mathrm{em}}\, W N_1, \tag{3.1}$$

where N_2 is the number of excited atoms, N_1 is the number of unexcited atoms and $N = N_1 + N_2$ is the total number of atoms. A, B_{em}, B_{ab} are the spontaneous emission rate, the stimulated emission rate and the absorption rate, respectively. In ordinary vacuum, the stimulated emission rate and the absorption rate are equal, $B_{\mathrm{ab}} = B_{\mathrm{em}} = B$, so that in steady-state conditions the ratio of the number of excited atoms with respect to the total number of atoms is given by

$$\frac{N_2}{N} = \frac{1}{2 + A/(B \cdot W)}. \tag{3.2}$$

Clearly, the magnitude of the excited atomic population per atom N_2/N, has an upper bound of $\frac{1}{2}$, and in the case of

ordinary vacuum implicitly prohibits positive values of the atomic inversion. As a result, coherent optical switching is not possible in this manner in ordinary vacuum. However, near a photonic band edge (or other sharp features in the density of states) the underlying basis for (3.1) is no longer valid. Fermi's golden rule for absorption and emission of light from the atom requires that the density of states in the electromagnetic reservoir is smooth and featureless. In a more detailed picture, the interaction of the external laser with the atom leads to a set of 'dressed atomic states' [44], which are displaced in frequency relative to the 'bare' atomic level. Equation (3.1) is no longer appropriate if the density of states exhibits significant variation on the frequency scale of the dressed atomic level shift. In fact we show in the following analysis that population inversion and other unusual effects can be achieved at relatively low coherent pumping thresholds, if the density of states 'discontinuity' is sufficiently large.

3.1. Model Hamiltonian

The rapid variations in the photonic density of states (DOS) with frequency in a PBG material lead to fundamental modifications in the response of a two-level system to an external laser field relative to ordinary vacuum. In this section we consider an effective mass approximation to the full dispersion relation of a photonic crystal. For a real dielectric crystal with an allowed point-group symmetry, the band edge occurs at certain points along the Bragg planes of the lattice and the electromagnetic dispersion relation may be approximated by $\omega(\boldsymbol{k}) = \omega_{\mathrm{C}} + A(\boldsymbol{k}-\boldsymbol{k}_0)^2$, where $\boldsymbol{k}_0$ is a point of the Brillouin zone boundary associated with the band edge. We consider a two-level atom interacting with a quantized electromagnetic field of a photonic crystal. In the rotating wave approximation (RWA) and in a frame of reference rotating with the atomic resonance frequency, ω_{A}, the Hamiltonian describing the total system is [29]

$$H = H_0 + H_{\mathrm{int}}, \tag{3.3a}$$

$$H_0 = \sum_{\lambda} \hbar \Delta_\lambda a_\lambda^\dagger a_\lambda, \tag{3.3b}$$

$$H_{\mathrm{int}} = \mathrm{i}\hbar \sum_{\lambda} g_\lambda \left(a_\lambda^\dagger \sigma_{12} - \sigma_{21} a_\lambda\right), \tag{3.3c}$$

where

$$g_\lambda = \frac{\omega_{\mathrm{A}} d_{21}}{\hbar}\left[\frac{\hbar}{2\epsilon_0 \omega_\lambda \mathcal{V}}\right]^{1/2} \boldsymbol{e}_\lambda \cdot \boldsymbol{u}_d,$$

and $\sigma_{ij} = |i\rangle\langle j|$ $(i, j = 1, 2)$ are the atomic pseudo-spin operators, $\sigma_3 = \sigma_{22} - \sigma_{11}$ describes the atomic inversion, a_λ and $a_\lambda^\dagger$ are the radiation field annihilation and creation operators and $\Delta_\lambda = \omega_\lambda - \omega_A$ represents the λ-mode detuning frequency from the atomic frequency. Here, the atomic-dipole moment $\boldsymbol{d}$ has been chosen to be real without loss of generality by a convenient choice of the atomic Hamiltonian eigenstates $|1\rangle$, $|2\rangle$ phases, with d_{21} its magnitude and $\boldsymbol{u}_d$ the unit vector. $\boldsymbol{e}_\lambda \equiv \boldsymbol{e}_{k,\sigma}$, with $\sigma = 1, 2$, are the transverse polarization vectors of the radiation field, and $\mathcal{V}$ is the quantization volume. We now consider that an external single-mode laser field drives the atomic system described above. The interaction Hamiltonian between the atom and the laser mode is $H_{\mathrm{AL}} = -\boldsymbol{d} \cdot \boldsymbol{E}_{\mathrm{L}}$, with $\boldsymbol{d} = \boldsymbol{d}_{21}\,(\sigma_{21} + \sigma_{12})$, the atomic electric dipole operator and $\boldsymbol{E}_{\mathrm{L}}$ the transverse electric field operator given by

$$\boldsymbol{E}_L = \mathrm{i}\sqrt{\frac{\hbar\omega_{\mathrm{L}}}{2\epsilon_0 \mathcal{V}}}\boldsymbol{e}_L\left(a_L - a_L^\dagger\right). \tag{3.4}$$

Here, $\boldsymbol{e}_L$ is the polarization of the laser field, ω_{L} the laser field frequency and a_L, $a_L^\dagger$, the annihilation and creation laser field operators. We also assume that the laser is in a coherent state $|\alpha \cdot \exp(-\mathrm{i}\omega_{\mathrm{L}} t)\rangle$, with $\alpha = |\alpha|\,\mathrm{e}^{-\mathrm{i}\phi_L}$, and that the occupation number of the laser mode $\overline{N}_{\mathrm{L}} = |\alpha^2|$ is high enough that we can disregard the influence of the atomic system on the laser field radiation and average over the laser field degrees of freedom. Under these assumptions, H_{AL} can be brought to the usual RWA form of the interaction between an two-level atom and a classical coherent monochromatic laser field

$$H_{\mathrm{AL}} = \hbar\varepsilon\left(\sigma_{21}\,\mathrm{e}^{-\mathrm{i}(\omega_{\mathrm{L}} t + \phi_T)} + \sigma_{12}\,\mathrm{e}^{\mathrm{i}(\omega_{\mathrm{L}} t + \phi_T)}\right).$$

Here, $\varepsilon = \boldsymbol{d}_{21} \cdot \boldsymbol{\mathcal{E}}/\hbar$ is the Rabi frequency, the laser electric field magnitude $|\boldsymbol{\mathcal{E}}| = \sqrt{\hbar\omega_{\mathrm{L}}/2\epsilon_0\mathcal{V}} \cdot \sqrt{\overline{N}_{\mathrm{L}}} e_L$, and all the phase contributions are grouped in $\phi_T = \phi_L - \pi/2$. We now couple the driven atomic system to the radiation reservoir of a photonic crystal. Using the notations introduced previously, the total Hamiltonian of the system is given by $H = H_0 + H_1$, where

$$H_0 = \sum_{\lambda} \hbar\omega_\lambda\, a_\lambda^\dagger a_\lambda + \tfrac{1}{2}\hbar\omega_A \sigma_3 + H_{\mathrm{AL}}, \tag{3.5a}$$

$$H_1 = \mathrm{i}\hbar \sum_{\lambda} g_\lambda\,(a_\lambda^\dagger \sigma_{12} - a_\lambda \sigma_{21}). \tag{3.5b}$$

In order to eliminate the explicit time dependence of the Hamiltonian, we transform to a rotating frame of reference with the frequency ω_{L}, via the unitary transformation

$$H'(t) = R^\dagger(t) H R(t) - R^\dagger(t)\frac{\mathrm{d}R(t)}{\mathrm{d}t},$$

where

$$R(t) = \exp\left[-\mathrm{i}\,(\omega_{\mathrm{L}} t + \phi_T)\left(\tfrac{1}{2}\sigma_3 + \sum_{\lambda} \hbar a_\lambda^\dagger a_\lambda\right)\right].$$

In the rotating frame of reference, the effective Hamiltonian becomes

$$H' = H_0' + H_1', \tag{3.6a}$$

$$H_0' = \sum_{\lambda} \hbar\Delta_\lambda\, a_\lambda^\dagger a_\lambda + \tfrac{1}{2}\hbar\Delta_{AL}\sigma_3 + \hbar\varepsilon\,(\sigma_{12} + \sigma_{21})\,, \tag{3.6b}$$

$$H_1' = \mathrm{i}\hbar \sum_{\lambda} g_\lambda\,(a_\lambda^\dagger \sigma_{12} - a_\lambda \sigma_{21}), \tag{3.6c}$$

with $\Delta_\lambda \equiv \omega_\lambda - \omega_{\mathrm{L}}$ and $\Delta_{\mathrm{AL}} \equiv \omega_{\mathrm{A}} - \omega_{\mathrm{L}}$. For simplicity, from now on we drop the prime sign on the Hamiltonian.

3.2. Heisenberg's equations of evolution; the dressed picture

To obtain the dressed states, we diagonalize the atom plus external field part of the total Hamiltonian. This is done by a unitary transformation to the dressed atomic basis, defined by $|\tilde{1}\rangle = c|1\rangle + s|2\rangle$, $|\tilde{2}\rangle = -s|1\rangle + c|2\rangle$, where $c = \cos\phi$, $s = \sin\phi$, $\sin\phi^2 = \frac{1}{2}[1 - \mathrm{sign}(\Delta_{\mathrm{AL}})/(4\epsilon^2/\Delta_{\mathrm{AL}}^2 + 1)^{1/2}]$ and $0 \leqslant \phi \leqslant \pi/2$. The corresponding dressed atomic operators,

$R_{ij} = |\tilde{i}\rangle\langle\tilde{j}|(i, j = 1, 2)$, $R_3 = R_{22} - R_{11}$, are related to the bare atomic operators by

$$\begin{aligned}\sigma_{12} &= csR_3 + c^2R_{12} - s^2R_{21}\\ \sigma_{21} &= csR_3 - s^2R_{12} + c^2R_{21}\\ \sigma_3 &= (c^2 - s^2)R_3 - 2cs(R_{12} + R_{21}).\end{aligned} \tag{3.7}$$

This transformation leads to the noninteracting dressed state Hamiltonian

$$H_0 = \hbar\Omega R_3 + \hbar\sum_\lambda \Delta_\lambda\, a_\lambda^\dagger a_\lambda, \tag{3.8}$$

with $\Omega = \left[\epsilon^2 + \Delta_{\mathrm{AL}}^2/4\right]^{1/2}$, the generalized Rabi frequency.

We define the time-dependent interaction picture Hamiltonian $\tilde{H}_1 = U^\dagger(t)H_1U(t)$, where the unitary operator $U(t)$ is given by $U(t) = \exp(-\mathrm{i}H_0t/\hbar)$. In this picture, the interaction Hamiltonian $\tilde{H}_1$ takes the form

$$\begin{aligned}\tilde{H}_1 = \mathrm{i}\hbar\Lambda\sum_\lambda g_\lambda\big[a_\lambda^\dagger\big(csR_3\,\mathrm{e}^{\mathrm{i}\Delta_\lambda t} + c^2R_{12}\,\mathrm{e}^{\mathrm{i}(\Delta_\lambda-2\Omega)t}\\ -s^2R_{21}\,\mathrm{e}^{\mathrm{i}(\Delta_\lambda+2\Omega)t}\big)\big] + \mathrm{h.c.}\end{aligned} \tag{3.9}$$

The dressed atomic operators in this interaction picture exhibit the time dependence given by $\tilde{R}_{12}(t) = R_{12}(0)\exp(-2\mathrm{i}\Omega t)$, $\tilde{R}_{21}(t) = R_{21}(0)\exp(2\mathrm{i}\Omega t)$ and $\tilde{R}_3(t) = R_3(0)$. Clearly, $\tilde{R}_3(t)$, $\tilde{R}_{12}(t)$ and $\tilde{R}_{21}(t)$ can be considered as source operators for the central component, left and right side-bands of the Mollow triplet at the frequencies ω_{L}, $\omega_{\mathrm{L}} - 2\Omega$ and $\omega_{\mathrm{L}} + 2\Omega$. Hereafter, we drop the tilde on the interaction picture operators. The Hamiltonian given by (3.9) generates the following equations of motion:

$$\begin{aligned}\frac{\mathrm{d}}{\mathrm{d}t}a_\lambda(t) &= g_\lambda\big\{csR_3\mathrm{e}^{\mathrm{i}\Delta_\lambda t} + c^2R_{12}\mathrm{e}^{\mathrm{i}(\Delta_\lambda-2\Omega)t}\\ &\quad -s^2R_{21}\mathrm{e}^{\mathrm{i}(\Delta_\lambda+2\Omega)t}\big\},\end{aligned} \tag{3.10a}$$

$$\begin{aligned}\frac{\mathrm{d}}{\mathrm{d}t}R_{21}(t) &= \sum_\lambda g_\lambda\big\{-2cs\,a_\lambda^\dagger R_{21}\,\mathrm{e}^{\mathrm{i}\Delta_\lambda t} + c^2\,a_\lambda^\dagger R_3\,\mathrm{e}^{\mathrm{i}(\Delta_\lambda-2\Omega)t}\\ &\quad +2csR_{21}a_\lambda\mathrm{e}^{-\mathrm{i}\Delta_\lambda t} + s^2R_3a_\lambda\mathrm{e}^{-\mathrm{i}(\Delta_\lambda+2\Omega)t}\big\},\end{aligned} \tag{3.10b}$$

$$\begin{aligned}\frac{\mathrm{d}}{\mathrm{d}t}R_3(t) &= -2\sum_\lambda g_\lambda\big\{s^2\,a_\lambda^\dagger R_{21}\,\mathrm{e}^{\mathrm{i}(\Delta_\lambda+2\Omega)t}\\ &\quad +c^2\,a_\lambda^\dagger R_{21}\,\mathrm{e}^{\mathrm{i}(\Delta_\lambda-2\Omega)t}\big\} + \mathrm{h.c.}\end{aligned} \tag{3.10c}$$

The field operators are eliminated by formally integrating (3.10*a*) and substituting the result back into (3.10*b*) and (3.10*c*). Further, we average over the field and atomic variables. We assume that the radiation field is initially in its vacuum state i.e. $\langle a_\lambda(0)\rangle = \langle a_\lambda^\dagger(0)\rangle = \langle a_\lambda(0)R_{ij}(t)\rangle = 0$.

In this analysis, we use a perturbative approach to describe the first-order non-Markovian corrections to the resonance fluorescence phenomena in PBG materials. The perturbation parameter is the coupling constant between the atomic system and the photonic reservoir associated with the dielectric structure. The magnitude of this coupling is directly related to the photonic DOS in the neighbourhood of the resonant atomic frequency ω_{A}. For the anisotropic model used in this section, the photonic DOS is continuous and finite over the entire spectral range of interest—in the effective mass approximation, the DOS of an anisotropic PBG material is given by

$$\rho(\omega) \propto \begin{cases}(\omega - \omega_{\mathrm{C}})^{1/2} & \text{if} \quad \omega \geqslant \omega_{\mathrm{C}}\\ 0 & \text{if} \quad \omega < \omega_{\mathrm{C}}\end{cases} \tag{3.11}$$

—and, remarkably, the spectral region surrounding the band edge frequency ω_{C}, which is associated with the most prominent non-Markovian effects, is characterized by a relatively low magnitude of the DOS and, implicitly, the dynamics of the atomic system can be analysed within the framework of a perturbation approach.

In the Born approximation, we retain terms up to the second order in coupling strength between the radiation reservoir of the photonic crystal and the atomic system, and replace

$$R_{ij}(t) \approx \mathrm{e}^{-\mathrm{i}L_0(t-t')}\big\{R_{ij}(t')\big\} \approx R_{ij}(t'). \tag{3.12}$$

It follows that in the Born approximation $\langle R_{ij}(t)R_{mk}(t')\rangle \approx \langle R_{ij}(t')R_{mk}(t')\rangle = \langle R_{ik}(t')\rangle\delta_{jm}$.

We introduce the memory functions $G_0(t - t') = \sum_\lambda g_\lambda^2\mathrm{e}^{-\mathrm{i}\Delta_\lambda(t-t')}$ and $G_\pm(t - t') = \sum_\lambda g_\lambda^2\mathrm{e}^{-\mathrm{i}(\Delta_\lambda\pm2\Omega)(t-t')}$. In general, the memory functions $G_0(t - t')$ and $G_\pm(t - t')$ are determined by the radiation field DOS. For a broad-band, smoothly varying DOS of the photonic reservoir (as in ordinary vacuum), the dependence of the memory functions on the external field can be ignored and the memory time associated with the photonic reservoir can be considered negligibly small (the Markovian approximation) and we simplify $G_0(t - t') = G_\pm(t - t') \approx (\gamma/2)\delta(t - t')$, where $\gamma = \omega_{\mathrm{A}}^3d_{21}^2/3\pi\epsilon_0\hbar c^3$ is the usual decay rate for spontaneous emission in the absence of the PBG materials. However, the DOS of the photonic crystals exhibits band edge and other Van Hove singularities as described in the introduction. In such a system with fast variations of the DOS in the spectral range given by $\{\omega_{\mathrm{L}}-2\Omega, \omega_{\mathrm{L}}+2\Omega\}$ (shown in figure 4), the distinctive memory functions introduced previously lead to qualitatively different behaviour from ordinary vacuum. The system of equations characterizing the evolution of the atomic operators is further simplified by making the secular approximation i.e. the fast-oscillating terms with frequencies 2 and 4Ω are discarded. This approximation is valid in the regime $\Omega > \beta_{\mathrm{A}}$, where β_{A}^{-1} is the characteristic time scale of the evolution of the atomic system. For the anisotropic model of PBG it is given by $\beta_{\mathrm{A}} = \omega_{\mathrm{A}}^2d_{21}^2/8\hbar\epsilon_0\pi^2A^{3/2}$ [24]. Under these assumptions, the temporal evolution of the atomic system is described by the following equations:

$$\begin{aligned}\frac{\mathrm{d}}{\mathrm{d}t}\langle R_{21}(t)\rangle &= -2c^2s^2\int_0^t \mathrm{d}t'\,G_0^*(t - t')\langle R_{21}(t')\rangle\\ &\quad -c^4\int_0^t \mathrm{d}t'\,G_+^*(t - t')\langle R_{21}(t')\rangle\\ &\quad -2c^2s^2\int_0^t \mathrm{d}t'\,G_0(t - t')\langle R_{21}(t')\rangle\\ &\quad -s^4\int_0^t \mathrm{d}t'\,G_-(t - t')\langle R_{21}(t')\rangle,\end{aligned} \tag{3.13a}$$

$$\begin{aligned}\frac{\mathrm{d}}{\mathrm{d}t}\langle R_3(t)\rangle &= -2c^4\int_0^t \mathrm{d}t'\,G_+(t - t')\langle R_{22}(t')\rangle\\ &\quad +2s^4\int_0^t \mathrm{d}t'\,G_-(t - t')\langle R_{11}(t')\rangle + \mathrm{h.c.}\end{aligned} \tag{3.13b}$$

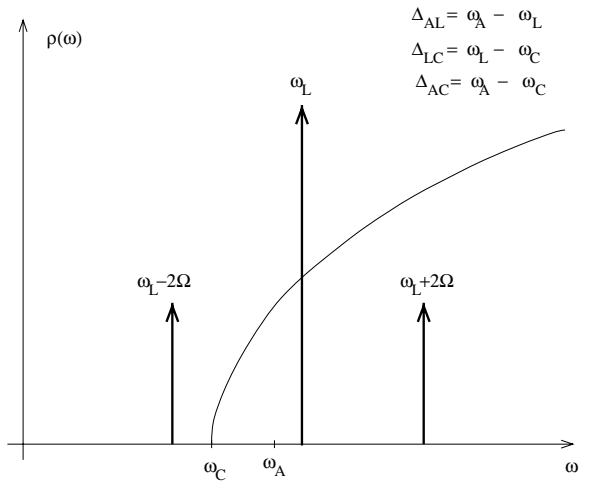

Figure 4. Relevant frequencies and frequency scales in the case of an anisotropic DOS. The laser frequency $\omega_{\rm L}$, and the atomic frequency, $\omega_{\rm A}$, are slightly positively detuned from the band edge frequency $\omega_{\rm C}$.

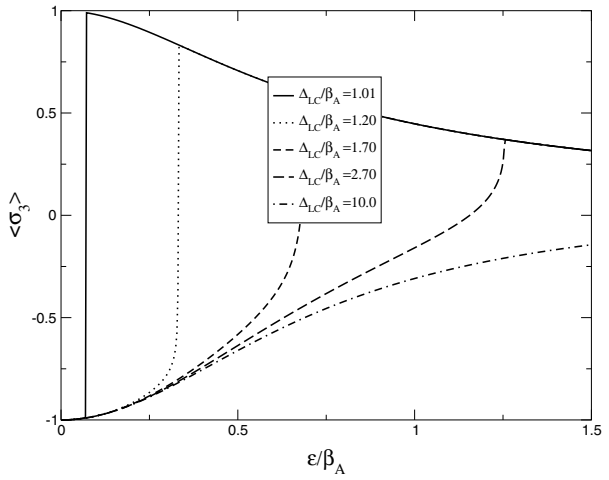

Figure 5. Atomic population inversion, $\langle\sigma_3\rangle$, as a function of the laser intensity $\epsilon/\beta_{\rm A}$ for different values of the laser frequency detuning: $\Delta_{\rm LC}/\beta_{\rm A} = 1.01$ (solid curve), $\Delta_{\rm LC}/\beta_{\rm A} = 1.20$ (dotted curve), $\Delta_{\rm LC}/\beta_{\rm A} = 1.70$ (dashed curve), $\Delta_{\rm LC}/\beta_{\rm A} = 2.70$ (long-dashed curve), $\Delta_{\rm LC}/\beta_{\rm A} = 10.0$ (dot–dashed curve). The atomic detuning is $\Delta_{\rm AL} = -\beta_{\rm A}$.

3.3. Switching by a moderate external field; the non-Markovian case

For weak and moderate external fields, the Mollow spectral components may remain close to the DOS discontinuity and it is necessary to solve equations (3.13*a*) and (3.13*b*) without any additional approximation such as the Markov approximation. For this purpose, we introduce the Laplace transforms of the atomic variables, $x(p) = \tilde{R}_3(p) = \mathcal{L}\{\langle R_3(t)\rangle\}$, $z(p) = \tilde{R}_{21}(p) = \mathcal{L}\{\langle R_{21}(t)\rangle\}$ and the memory functions $\tilde{G}_0(p) = \mathcal{L}\{G_0(t)\}$, $\tilde{G}_+(p) = \mathcal{L}\{G_+(t)\}$, $\tilde{G}_-(p) = \mathcal{L}\{G_-(t)\}$, where $\tilde{f}(p) = \mathcal{L}\{f(t)\} = \int_0^\infty \mathrm{e}^{-pt} f(t)$. With these notations, the solution of the evolution equations is given by

$$x(p) = \frac{x_0 p + [s^4\tilde{G}_-(p) - c^4\,\tilde{G}_+(p) + \text{c.c.}]}{p\,\{p + [c^4\,\tilde{G}_+(p) + s^4\tilde{G}_-(p) + \text{c.c}]\}}, \tag{3.14a}$$

$$z(p) = \frac{z_0}{p + c^4\tilde{G}_+^*(p) + s^4\tilde{G}_-(p) + 2c^2s^2[\tilde{G}_0(p) + \tilde{G}_0^*(p)]} \tag{3.14b}$$

where $x_0 = \langle R_3(0)\rangle$ and $z_0 = \langle R_{21}(0)\rangle$. In the Laplace space, the evolution of the dressed atomic population and polarization satisfy the system (3.14*a*) and (3.14*b*).

The time-dependent dressed atomic variables are given by the inverse Laplace transformation $\langle R_3(t)\rangle = \mathcal{L}^{-1}\{x(p)\}$, $\langle R_{21}(t)\rangle = \mathcal{L}^{-1}\{z(p)\}$, where

$$\mathrm{f}(t) = \mathcal{L}^{-1}\{\tilde{f}(p)\} = \frac{1}{2\pi\mathrm{i}}\int_{\varepsilon-i\infty}^{\varepsilon+i\infty} \mathrm{d}p\,\mathrm{e}^{pt}\,\tilde{f}(p).$$

Here, the real number ε is chosen such that $p = \varepsilon$ lies to the right of all singularities (poles and branch points) of the function to be integrated. The equations (3.14*a*) and (3.14*b*) are simplified by scaling the time variable by $\beta_{\rm A}^{-1}$ (the frequency is then scaled with $\beta_{\rm A}$). We numerically evaluate the inverse Laplace transforms of the atomic variables using an Adams algorithm [45]. Once the Laplace inversion is performed, the bare-state atomic averages are obtained through (3.7).

In ordinary vacuum, the atomic system does not exhibit steady-state inversion. Consequently (as argued in section 3), conventional lasers require additional atomic levels to achieve atomic inversion. In the PBG material, for a given intensity of the laser field, the atomic system reaches positive inversion (figures 5 and 6); if the jump in the photonic DOS is quite large, the atomic system achieves nearly total inversion. This behaviour is a consequence of the fact that the dressed state $|\tilde{1}\rangle$ (the left Mollow side-band at the frequency $\omega_{\rm L} - 2\Omega$) is placed in the spectral region with a low DOS and with slow decay, whereas the dressed state $|\tilde{2}\rangle$ (the right Mollow side-band at the frequency $\omega_{\rm L} + 2\Omega$) experiences a large DOS and a rapid decay. In the long-time limit, the population in the dressed state $|\tilde{1}\rangle$ is much larger than the atomic population in the dressed state $|\tilde{2}\rangle$. This imbalance of the atomic population between the dressed states is responsible for the atomic inversion in the bare picture. The derivation of a steady-state solution for the atomic inversion is facilitated by the identity $\lim_{t\to\infty}\{F(t)\} = \lim_{p\to 0}\{p\cdot\tilde{f}(p)\}$. Since $z(p)$ and $x(p)$ have only complex (not purely imaginary) poles it follows that the steady-state dressed atomic polarization vanishes. However, the dressed excited atomic inversion $\langle R_3\rangle^{\rm st} = \lim_{t\to\infty}\langle R_3(t)\rangle$ has a nontrivial behaviour

$$\langle R_3\rangle^{\rm st} = \begin{cases} -1 & \text{if} \quad \Delta_{\rm LC} \leqslant 2\Omega \\ \dfrac{s^4 - c^4\sqrt{(\Delta_{\rm LC}+2\Omega)\,/\,(\Delta_{\rm LC}-2\Omega)}}{s^4 + c^4\sqrt{(\Delta_{\rm LC}+2\Omega)\,/\,(\Delta_{\rm LC}-2\Omega)}} & \\ \text{if} \quad \Delta_{\rm LC} > 2\Omega & \end{cases} \tag{3.15}$$

where $\Delta_{\rm LC} = \omega_{\rm L} - \omega_{\rm C}$.

We check the consistency of the solution in two limiting cases. First, if we place the Mollow spectral components far outside the gap $\Delta_{\rm LC} \gg 2\Omega$, the system reaches the ordinary vacuum behaviour

$$\langle R_3\rangle^{\rm st} = -\frac{c^4 - s^4}{c^4 + s^4} \Longrightarrow \langle\sigma_{22}\rangle^{\rm st} = -\frac{(c^2 - s^2)^2}{c^4 + s^4}. \tag{3.16}$$

This limiting case is consistent with the Markovian approach (far away from the DOS singularity the photonic crystal

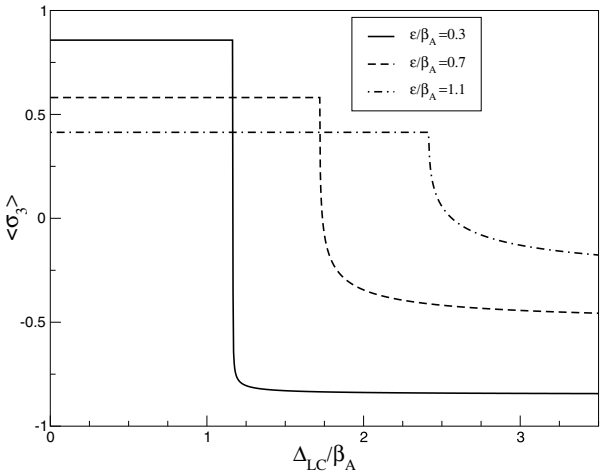

Figure 6. Atomic inversion $\langle\sigma_3\rangle$, as a function of the laser frequency detuning $\Delta_{\rm LC}/\beta_{\rm A}$ for different values of the laser intensity: $\epsilon/\beta_{\rm A} = 0.3$ (solid curve), $\epsilon/\beta_{\rm A} = 0.7$ (dashed curve), $\epsilon/\beta_{\rm A} = 1.1$ (dot-dashed curve). The atomic detuning is $\Delta_{\rm AL} = -\beta_{\rm A}$.

reservoir of modes is a Markovian reservoir). On the other hand, if we place the left spectral components inside the gap $\Delta_{\rm LC} < 2\Omega$, the atomic system becomes trapped in the $|\tilde{1}\rangle$ state:

$$\langle R_3\rangle^{\rm st} = -1 \implies \langle\sigma_{22}\rangle^{\rm st} = s^2 - c^2. \tag{3.17}$$

Consider a near-resonant laser excitation ($\omega_{\rm L} \approx \omega_{\rm A}$). If we begin with an atom with resonant transition frequency, $\omega_{\rm A}$, just outside the PBG (say, for instance, $\Delta_{\rm AC} \equiv \omega_{\rm A} - \omega_{\rm C} > 0$), it is possible to drive the system through the transition described above, simply by increasing the applied field intensity. For a nearly resonant laser excitation ($\omega_{\rm L} \approx \omega_{\rm A}$), the left Mollow side-band (at frequency $\omega_{\rm A} - 2\Omega$) passes through the photonic band edge frequency when $\Omega_{\rm crit} = \Delta_{\rm LC}/2$, while the other Mollow spectral components remain outside the gap. At this critical laser intensity, the atomic population exhibits switching from a noninverted state to an inverted state. In the bare picture, the atomic inversion can be expressed as

$$\langle\sigma_{22}\rangle^{\rm st} = \begin{cases} s^2 - c^2 & \text{if} \quad \Delta_{\rm LC} \leqslant 2\Omega \\ (c^2 - s^2)\,\dfrac{s^4 - c^4\sqrt{\frac{\Delta_{\rm LC}+2\Omega}{\Delta_{\rm LC}-2\Omega}}}{s^4 + c^4\sqrt{\frac{\Delta_{\rm LC}+2\Omega}{\Delta_{\rm LC}-2\Omega}}} & \text{if} \quad \Delta_{\rm LC} > 2\Omega. \end{cases} \tag{3.18}$$

It is apparent from figure 5 that for moderate values of the laser intensity, the atomic system switches very sharply from the ground state to the excited state, at a critical value of ϵ. This switching behaviour is caused by the very sensitive dependence of the dressed atomic population on the relative position of the Mollow spectrum components. The magnitude of the effect depends on the actual value of the laser detuning with respect to the band edge frequency $\Delta_{\rm LC} = \omega_{\rm L} - \omega_{\rm C}$. This interplay between the control parameters is shown in figure 6, where now the atomic population displays sharp switching behaviour as a function of the detuning of the laser field frequency for various choices of the applied laser field intensity. A stronger switching behaviour is presented in the next section in the context of collective behaviour of an ensemble of two-level atoms placed in a PBG material treated in a Markov approximation. In this case, there is further collective enhancement of the switching [25]. In particular, we show that the width of the switching region as measured by the change in pump intensity required to switch from absorption to gain is of order $1/N$ where N is the number of atoms in a cubic wavelength. This provides very large differential gain.

3.4. The influence of dephasing interactions and nonradiative relaxation

In order to make closer contact with experiment, we include phenomenological decay rates, $1/T_1^{\rm nr}$ and $1/T_2$, associated with other (nonradiative) decay and dephasing, respectively. Deep inside the gap, where radiative decay is negligible, the nonradiative contribution may become very important. In this case, $T_1^{\rm nr}$ and T_2 may be considered as empirical constants. The nonradiative decay may come from phonon assisted transitions, if the atom is placed in a solid matrix. Dephasing occurs if an atomic vapour is placed in the photonic crystal voids and is collisionally perturbed by the other atoms. If the atom is implanted in the dielectric region, the interaction with lattice vibrations of the host dielectric material (elastic scattering of the phonons on the atomic system) will cause dephasing. The effect of these additional decay and dephasing mechanisms was calculated in [29]. Here, we present only the steady-state results for the dressed atomic population inversion and polarization

$$\langle R_3\rangle^{\rm st} = \begin{cases} \Big[-2c^4\sqrt{\Delta_{\rm LC}+2\Omega} + \left(s^2-c^2\right)/\tilde{T}_1^{\rm nr}\Big] \\ \times\Big[2c^4\sqrt{\Delta_{\rm LC}+2\Omega} + 4s^2c^2/\tilde{T}_2 \\ +\left(s^2-c^2\right)^2/\tilde{T}_1^{\rm nr}\Big]^{-1} & \text{if} \quad \Delta_{\rm LC} \leqslant 2\Omega, \\ \Big[2s^4\sqrt{\Delta_{\rm LC}-2\Omega} - 2c^4\sqrt{\Delta_{\rm LC}+2\Omega} \\ +\left(s^2-c^2\right)/\tilde{T}_1^{\rm nr}\Big] \\ \times\Big[2s^4\sqrt{\Delta_{\rm LC}-2\Omega} + 2c^4\sqrt{\Delta_{\rm LC}+2\Omega} + 4s^2c^2/\tilde{T}_2 \\ +\left(s^2-c^2\right)^2/\tilde{T}_1^{\rm nr}\Big]^{-1} & \text{if} \quad \Delta_{\rm LC} > 2\Omega, \end{cases} \tag{3.19}$$

where we introduced the scaled nonradiative decay and dephasing parameters $\tilde{T}_1^{\rm nr} = T_1^{\rm nr}\cdot\beta_{\rm A}$, and $\tilde{T}_2 = T_2\cdot\beta_{\rm A}$, respectively.

Clearly, the additional decay and dephasing mechanisms tend to weaken the switching effect. The robustness of the switching effect follows from an estimate of the timescale factor in PBG materials. In the case of the anisotropic model of the PBG, the timescale factor $\beta_{\rm A}$ can be expressed as

$$\beta_{\rm A} = \omega_C\,\frac{1}{\tilde{A}^3}\,\frac{9}{256\pi}\left(\frac{\gamma}{\omega_{21}}\right)^2,$$

where we introduced the dimensionless constant $\tilde{A} = A/(c^2\,\omega_C)$ (see section 3.1) and γ is the corresponding free space spontaneous emission rate. The values of $\omega_{\rm C}$, and $\tilde{A}$, are determined by the specifics of the dielectric structure considered, and we obtain a very strong dependence on the curvature of the dispersion relation. Moreover, real band structure calculations show an extremely sensitive dependence

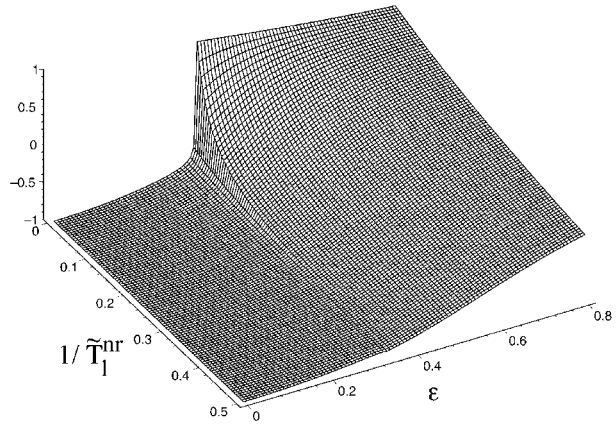

Figure 7. Atomic population inversion $\langle\sigma_3\rangle$, as a function of ϵ/β_A and the nonradiative decay rate $1/\tilde{T}_1^{nr}$ in the absence of the phonon-mediated dephasing, $1/T_1 \to 0$. The laser field frequency detuning is $\Delta_{LC}/\beta_A = 1.2$, $\Delta_{AL}/\beta_A = -1$, and $\Delta_{AC}/\beta_A = 0.2$.

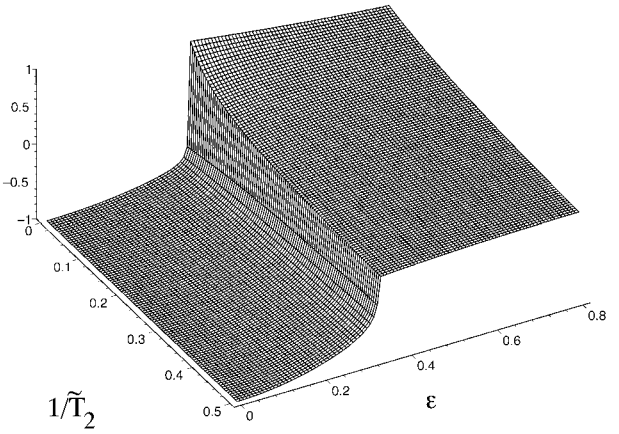

Figure 8. Atomic population inversion $\langle\sigma_3\rangle$, as a function of ϵ/β_A and the nonradiative dephasing rate $1/\tilde{T}_2$. The laser field frequency detuning is $\Delta_{LC}/\beta_A = 1.2$, $\Delta_{AL}/\beta_A = -1$, and $\Delta_{AC}/\beta_A = 0.2$.

of the curvature of the dispersion relation on the specific direction in the reciprocal space $\boldsymbol{k}_0$, and produce a wide range of values for the dimensionless parameter $\tilde{A}$. We are using in our numerical estimations a timescale factor range $0.8\gamma \leqslant \beta_A \leqslant 10\gamma$, but point out that a more accurate estimation has to be obtained by using band structure calculations for a real photonic crystal.

Clearly, as shown in figures 7 and 8, a sizable switching effect is present even when $1/\tilde{T}_1^{nr}$, $1/\tilde{T}_2 \approx 1$. It is also apparent that the nonradiative decay contribution (figure 7) is much more deleterious to switching effects than the dephasing mechanisms (figure 8).

4. Collective atomic switching in photonic bandgap materials

In this section we analyse the atomic population inversion and the statistics of a system of two-level atoms driven by an external laser field in a photonic crystal [25, 46]. For large deviations of the mode density between the components of the scattered radiation spectrum (Mollow spectrum) [44], the inversion in the atomic population occurs at low threshold and for a large total number of the atoms in cubic wavelength, $N \gg 1$, the collective switching from the ground state and the excited state occurs over a very narrow range of intensity of the driven laser field. Furthermore, under certain conditions, the excited atoms exhibit strong sub-Poissonian statistics and the switching speed exhibits a collective enhancement proportional to N^2. This suggests additional applications to fast optical switching devices, sub-Poissonian pumping for lasers [25,47,48] and 'noiseless' all-optical transistors (which preserve the input signal-to-noise ratio). In our theoretical treatment we limit ourselves to a 'point interaction'; i.e., the spatial extent of the active region of the PBG material is less then the wavelength of the emitted radiation. We assume that the concentration of the active atoms belongs to an intermediate regime, high enough to fulfill the 'point' model, but small enough to allow us to neglect direct interaction between different atomic dipoles.

4.1. The system description

The coupling between the atomic system and the multi-mode radiation field of the PBG causes both energy loss and damping of the atomic polarization. The polarization damping is due to the phase randomization of the atomic wavefunctions by thermal and vacuum fluctuations of the electromagnetic field of the reservoir (the overlap between the ground- and excited-state wavefunction decays in time) [49]. Moreover, as seen in the single-atom case, it is necessary to take into account the additional dephasing that arises from atomic collisions and elastic scattering of the phonons of the host-confined photonic material. In the interaction picture and in a rotating frame of reference (rotating with the laser field frequency ω_L) the Hamiltonian has the form $H = H_0 + H_1 + H_{deph}$, with

$$H_0 = \tfrac{1}{2}\hbar\Delta_{AL}J_3 + \hbar\epsilon\,(J_{12} + J_{21}) + \sum_\lambda \hbar\Delta_\lambda a_\lambda^\dagger a_\lambda,$$
$$H_1 = \mathrm{i}\hbar\sum_\lambda g_\lambda\big(a_\lambda^\dagger J_{12} - J_{21}a_\lambda\big), \tag{4.1}$$

where now $J_{ij} = \sum_{k=1,N}|i\rangle_k\langle j|_k$ $(i, j = 1, 2)$ are the *collective* atomic operators, $J_3 = J_{22} - J_{11}$ is the atomic operator describing the population inversion, $\Delta_{AL} = \omega_A - \omega_L$, $\Delta_\lambda = \omega_\lambda - \omega_L$ and ω_A, ω_L, ω_λ represent the atomic resonant frequency, the applied laser field frequency and the frequency of a mode λ, respectively. The Hamiltonian, H_{deph}, accounts for the additional nonradiative interactions mentioned before.

The collective atomic operators can be expressed using the Schwinger (bosonic) representation $J_{ij} = a_i^\dagger a_j$, $i, j = 1, 2$ and $a_i^\dagger$, a_j are the bosonic creation and annihilation operators of atoms in the states $|i\rangle$, $|j\rangle$. The usual bosonic commutation relations are modified by the constraint that the total number of atoms is fixed, i.e. $a_i^\dagger a_1 + a_2^\dagger a_2 = J_{11} + J_{22} = N$. The Hamiltonian part that describes the atom–applied field system can be diagonalized by means of the dressed state transformation defined earlier for a single atom. Defining the dressed state collective operators $R_{ij} \equiv \sum_{k=1}^N |\tilde{i}\rangle_{kk}\langle\tilde{j}|$, we obtain $H_0 = \hbar\Omega\,R_3 + \sum_\lambda \hbar\Delta_\lambda a_\lambda^\dagger a_\lambda$, while the interaction Hamiltonian H_1, can be cast in the form

$$H_1 = \mathrm{i}\hbar\sum_\lambda g_\lambda\big(\tfrac{1}{2}\sin 2\phi\, a_\lambda^\dagger R_3\,\mathrm{e}^{\mathrm{i}\,\Delta_\lambda t} + \cos^2\phi\, a_\lambda^\dagger R_{21}\,\mathrm{e}^{\mathrm{i}\,(\Delta_\lambda - 2\Omega)t}$$

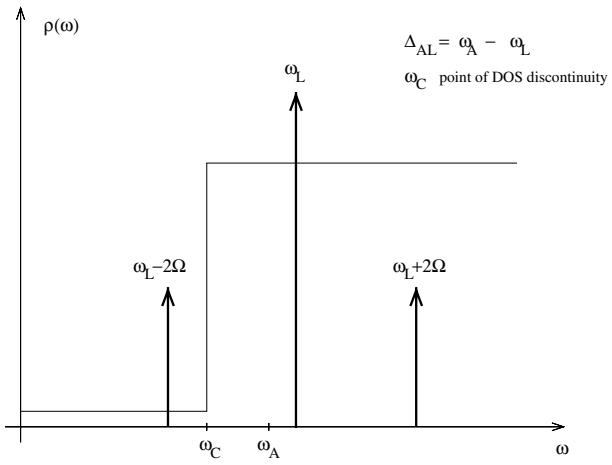

Figure 9. Relevant frequencies and frequency scales in the case of a steplike DOS.

$$-\sin^2\phi\, a_\lambda^\dagger R_{21}\, \mathrm{e}^{\mathrm{i}\,(\Delta_\lambda+2\Omega)t}\big) + \text{h.c.} \tag{4.2}$$

where $R_3 = R_{22} - R_{11}$. The Hamiltonian H_{deph} transforms similarly, by replacing J_3, J_{12}, J_{21} with

$$\begin{aligned} J_{12} &= 1/2 \sin 2\phi\, R_3 + \cos^2\phi R_{12}\, \mathrm{e}^{-2\mathrm{i}\Omega t} - \sin^2\phi\, R_{21}\, \mathrm{e}^{2\mathrm{i}\Omega t} \\ J_{21} &= 1/2 \sin 2\phi\, R_3 + \cos^2\phi R_{21}\, \mathrm{e}^{2\mathrm{i}\Omega t} - \sin^2\phi\, R_{12}\, \mathrm{e}^{-2\mathrm{i}\Omega t} \\ J_3 &= \cos 2\phi\, R_3 - \sin 2\phi\big(R_{12}\, \mathrm{e}^{-2\mathrm{i}\Omega t} + R_{21}\, \mathrm{e}^{2\mathrm{i}\Omega t}\big). \end{aligned} \tag{4.3}$$

4.2. The master equation formalism

The collective spectral and statistical properties of the Mollow spectrum in free space are well known [50]. In the photonic crystal we shall assume that the photonic density of modes at the atomic frequency exhibits some singularity (a step discontinuity for instance) so that the Mollow spectral components experience very different photonic mode densities. The model is simplified under the assumption that the photonic DOS, while singular at a given frequency, is constant over the spectral regions surrounding the dressed-state frequencies ω_{L}, $\omega_{L-2\Omega}$, $\omega_{L+2\Omega}$, as depicted in figure 9.

In these conditions, the usual formalism of open systems can be employed to obtain the master equation. We assume that the radiative and the dephasing reservoirs are statistically independent, such that we can evaluate separately their contributions to the master equation describing the temporal evolution of the atomic system. We consider the interaction between the atomic system and the reservoirs to be turned on at $t = 0$ (initially, there are no correlations between the system and the reservoir) and make the Born approximation (discard terms containing contributions higher than second order in the atomic system–reservoir interaction) and obtain, in the interaction picture, the following general equation of evolution [49]:

$$\left[\frac{\partial\tilde\rho(t)}{\partial t}\right]_{\text{rad}} = -1/\hbar^2 \times \int_0^t \mathrm{d}t'\ \mathrm{tr}_{\text{R}}\{[\tilde H_{\text{SR}}(t), [\tilde H_{\text{SR}}(t'), \tilde\rho(t')R_0]]\}. \tag{4.4}$$

Here, $\tilde\rho(t)$ is the reduced density operator of the atomic system (obtained after a trace tr_{R} has been performed over the reservoir degrees of freedom). $H_{\text{SR}}(t)$ represents a generic interaction Hamiltonian between the atomic system and the reservoir (in our analysis H_{SR} is given by (4.2)). R_0 is the initial density operator of the reservoir (the reservoir state is assumed to be virtually unchanged by the its coupling to the atomic system), which for simplicity is considered to be the vacuum state. The modal DOS depicted in figure 9 allows us to make a simplifying Markov approximation, in which we replace $\tilde\rho(t')$ by $\tilde\rho(t)$ in (4.4). Since the DOS is smooth and featureless in the vicinity of the individual Mollow sidebands, it is possible to associate spontaneous emission rates γ_0 and $\gamma_\pm$ with each of the frequencies ω_{L} and $\omega_{\text{L}} \pm 2\Omega$. If on the other hand, the external laser field intensity (Rabi frequency) Ω was very small, it would be necessary to incorporate the non-Markovian radiative dynamics associated with the DOS discontinuity. Non-Markovian collective dynamics is beyond the scope of this paper. However as suggested by our single-atom switching analysis in section 3, we can anticipate that non-Markovian effects will lead to more robust and lower-threshold collective switching behaviour. Moreover, we neglect the small energy shifts caused by atom–reservoir interaction, and discard the fast-oscillating terms with frequencies $\pm2\Omega$, $\pm4\Omega$ in the expansion of the H_{SR} and the double commutator. This secular approximation is valid for moderate applied laser fields, such that $\Omega \gg N\gamma_{0,\pm}$. However, the qualitative picture that emerges is valid even in the absence of this simplifying approximation.

The radiative part of the master equation for the atomic system, in the 'dressed' atomic basis, is then given by [49]

$$\begin{aligned} \left[\frac{\partial\tilde\rho(t)}{\partial t}\right]_{\text{rad}} &= \frac{\gamma_0}{2}\sin^2\phi\cos^2\phi\cdot\big(R_3\tilde\rho R_3 - R_3^2\tilde\rho\big) \\ &+\frac{\gamma_-}{2}\sin^4\phi\cdot\big(R_{12}\tilde\rho R_{21} - R_{21}R_{12}\tilde\rho\big) \\ &+\frac{\gamma_+}{2}\cos^4\phi\cdot\big(R_{12}\tilde\rho R_{21} - R_{21}R_{12}\tilde\rho\big) + \text{h.c.}, \end{aligned} \tag{4.5}$$

where $\gamma_0 = \sum_\lambda g_\lambda^2\ \delta(\omega_\lambda - \omega_{\text{L}})$ and $\gamma_\pm = \sum_\lambda g_\lambda^2\ \delta(\omega_\lambda - \omega_{\text{L}} \mp 2\Omega)$. The master equation that we obtained reduces to the free space case for $\gamma_- = \gamma_+ = \gamma_0$ [51]. The same analysis applied to the dephasing interaction and the dephasing part of master equation, in the 'bare' atomic basis, yields

$$\left[\frac{\partial\tilde\rho(t)}{\partial t}\right]_{\text{deph}} = \frac{\gamma_{\text{p}}}{2}\big[J_3\tilde\rho J_3 - J_3^2\,\tilde\rho\big] + \text{h.c.} \tag{4.6}$$

Here, we introduced a phenomenological dephasing rate γ_{p} (its exact value is dependent on the DOS of the specific dephasing reservoir considered). Using the transformation of the bare collective atomic operators to the dressed-state collective operators, the 'dressed' dephasing part of the master equation can be cast in the form

$$\begin{aligned} \left[\frac{\partial\tilde\rho(t)}{\partial t}\right]_{\text{deph}} &= \frac{\gamma_{\text{p}}}{2}\cos^2(2\phi)\cdot\big(R_3\tilde\rho R_3 - R_3^2\,\tilde\rho\big) \\ &+\frac{\gamma_{\text{p}}}{2}\sin^2(2\phi)\cdot\big(R_{21}\tilde\rho R_{12} - R_{12}R_{21}\tilde\rho\big) \\ &+\frac{\gamma_{\text{p}}}{2}\sin^2(2\phi)\cdot\big(R_{12}\tilde\rho R_{21} - R_{21}R_{12}\tilde\rho\big) + \text{h.c.} \end{aligned} \tag{4.7}$$

4.3. The system analysis

Altogether, the dressed-state master equation for the density operator in the Born–Markov approximations (using the secular approximation) has the form

$$\frac{\partial\tilde{\rho}(t)}{\partial t} = \frac{A_0}{2}\left(R_3\,\tilde{\rho}\,R_3 - R_3^2\,\tilde{\rho}\right) + \frac{A_-}{2}\left(R_{21}\,\tilde{\rho}\,R_{12} - R_{12},\,R_{21}\,\tilde{\rho}\right) + \frac{A_+}{2}\left(R_{12}\,\tilde{\rho}\,R_{21} - R_{21}R_{12}\tilde{\rho}\right) \tag{4.8}$$

where $A_0 \equiv \gamma_0 \sin^2\phi\cos^2\phi + \gamma_\mathrm{p}\cos^2(2\phi)$, $A_- \equiv \gamma_-\sin^4\phi + \gamma_\mathrm{p}\sin^2(2\phi)$ and $A_+ \equiv \gamma_+\cos^4\phi + \gamma_\mathrm{p}\cos^2(2\phi)$. We map the master equation using the dressed-state ket vector basis $\{|n\rangle\}_n = \{|N-n, n\rangle\}_n$, which describes symmetrized N-atom states, in which $N-n$ atoms are in the lower dressed state $|\tilde{1}\rangle$, and n atoms are excited in the upper state $|\tilde{2}\rangle$. The dressed-state ket vector is analogous to the angular momentum eigenvector with total angular momentum $J = N$, and projection $M = (2n - N)$. Using the bosonic representation of the dressed collective atomic operators, their action on the basis vectors is given by

$$\begin{aligned} R_{12}\,|n\rangle &= \sqrt{n\,(N-n+1)}\,|n-1\rangle \\ R_{21}\,|n\rangle &= \sqrt{(N-n)\,(n+1)}\,|n+1\rangle \\ R_3\,|n\rangle &= (2n-N)|n\rangle. \end{aligned} \tag{4.9}$$

In this basis, the diagonal matrix elements of the density operator, $P_n = \langle n|\rho|n\rangle = \rho_{n,n}$, satisfy the equation

$$\frac{\partial P_n}{\partial t} = n(N-n+1)\left[A_-P_{n-1} - A_+P_n\right] - (n+1)\,(N-n)\left[A_-P_n - A_+P_{n+1}\right]. \tag{4.10}$$

In the steady-state limit, $\dot{\tilde{\rho}} = 0$, the off-diagonal elements of the density matrix vanish, and the diagonal ones obey the equation

$$n(N-n+1)\left[A_-P_{n-1} - A_+P_n\right] - (n+1)\,(N-n)\left[A_-P_n - A_+P_{n+1}\right] = 0 \tag{4.11}$$

which can be cast in the form $f(n) = f(n-1)$ where the function $f(n)$ is given by

$$f(n) = (n+1)\,(N-n)\left[A_-P_n - A_+P_{n+1}\right]. \tag{4.12}$$

Clearly, $f(n)$ has to be independent of n. It follows that the solution for $P(n)$ takes a simple form $P_n = P_0\,\xi^n$, with $\xi = A_-/A_+$. Here, P_0 is obtained from the normalization condition $\sum_{n=0}^{N} P_n = 1$, as $P_0 = 1/Z$, with $Z = \sum_{n=0}^{N}\xi^n = \left(\xi^{N+1}-1\right)/(\xi-1)$, analogous to a partition sum. With the atomic distribution function P_n determined, we can evaluate

$$\begin{aligned} \langle n\rangle &= \sum_{n=0}^{N} n\,P_n = \xi\frac{\partial}{\partial\xi}\ln(Z) \\ &= \frac{N\xi^{N+2} - (N+1)\xi^{N+1} + \xi}{(\xi-1)^2} \\ &= \frac{(N+1)\,\xi^{N+1}}{\xi^{N+1}-1} - \frac{\xi}{\xi-1} \end{aligned} \tag{4.13a}$$

$$\begin{aligned} \langle n^2\rangle &= \sum_{n=0}^{N} n^2 P_n = \xi^2\frac{\partial^2}{\partial\xi^2}\ln(Z) + \xi^2\left(\frac{\partial}{\partial\xi}\ln(Z)\right)^2 \\ &\quad + \xi\frac{\partial}{\partial\xi}\ln(Z) \\ &= \left(N^2\xi^{N+3} - (2N^2+2N-1)\xi^{N+2} + (N+1)^2\xi^{N+1}\right. \\ &\quad \left. -\xi^2 - \xi\right)\left\{(\xi-1)^2\left(\xi^{N+1}-1\right)\right\}^{-1}. \end{aligned} \tag{4.13b}$$

The dependence of the mean number of atoms in the excited dressed state $|\tilde{2}\rangle$ on the parameter ξ is of central importance in our analysis. To obtain more insight into this dependence, let us analyse the case in which the number of atoms becomes very large, $N \gg 1$. The parameter space of ξ is scanned first for the case $\xi \neq 1$ (in particular, for $|\xi - 1| \gg 1/N$). In these conditions, the mean number of atoms in the dressed excited state is given by

$$\langle n\rangle \overset{N\to\infty}{\longrightarrow} \begin{cases} N - 1 - \xi/(\xi-1) & \text{if} \quad \xi > 1 \\ \xi/(\xi-1) & \text{if} \quad \xi < 1 \end{cases} \tag{4.14}$$

whereas if $\xi = 1$

$$\langle n\rangle \overset{N\to\infty}{\Longrightarrow} \frac{1}{Z}\sum_{n=0}^{N} n = \frac{1}{N+1}\left[\frac{N(N+1)}{2}\right] = \frac{N}{2}. \tag{4.15}$$

It is clear that $\xi = 1$ constitutes a critical point of the problem. Below this critical point, the number of atoms in the excited dressed state $|\tilde{2}\rangle$ is independent of the total number of atoms, whereas above this threshold value, the number of dressed excited atoms becomes directly proportional to the total number of atoms in the system (4.14). As shown in figure 10, the dressed-state population undergoes a 'phase transition' at $\xi \approx 1$, characterized by a collective switching of the dressed atoms from the ground state to the excited state. The width of the transition region is of order $\mathcal{O}(1/N)$, which implies that for a large number of atoms, the switching effect is extremely sudden (i.e. the required variation in the intensity of the external driving field is extremely small). The collective switching occurs provided that the function $\xi(\epsilon)$ crosses unity as a function of the applied field intensity. We can rewrite ξ in the form

$$\xi = A_-/A_+ = \left(\gamma_-/\gamma_+\sin^4\phi + \gamma_\mathrm{p}/\gamma_+\sin^2 2\phi\right) \times \left(\cos^4\phi + \gamma_\mathrm{p}/\gamma_+\sin^2 2\phi\right)^{-1}. \tag{4.16}$$

Let us assume that the resonant atomic transition is negatively detuned with respect to the applied laser frequency, i.e. $\Delta_\mathrm{AL} \equiv \omega_\mathrm{A} - \omega_\mathrm{L} < 0$, and $\sin\phi^2 = \frac{1}{2}[1 + 1/(1 + 4\epsilon^2/\Delta_\mathrm{AL}^2)^{1/2}]$. Under these assumptions, the necessary condition for $\xi(\epsilon)$ to pass through unity (as a function of pump laser amplitude ϵ) is that $\gamma_-/\gamma_+ < 1$. This requires that the left side-band component of the Mollow spectrum is placed in the spectral region characterized by a low DOS (which will correspond to a gap or pseudo-gap of the PBG material). In the opposite case, when the resonant atomic transition is positively detuned with respect to the applied laser frequency $\Delta_\mathrm{AL} \equiv \omega_\mathrm{A} - \omega_\mathrm{L} > 0$, the necessary condition for achieving switching becomes $\gamma_-/\gamma_+ < 1$, which corresponds to a mirror image of the negative-detuning case.

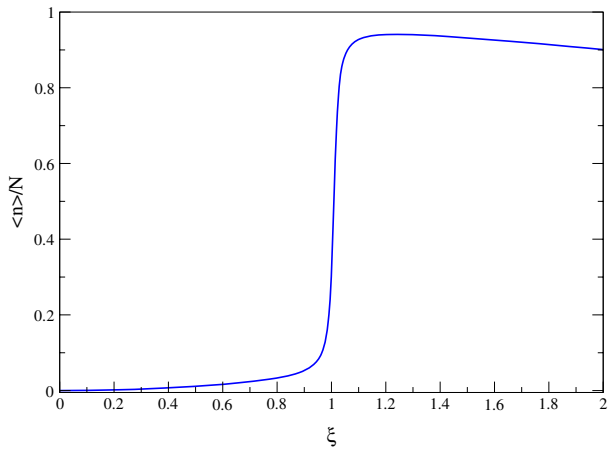

Figure 10. Typical behaviour of the average number of atoms in the dressed excited state $|\tilde{2}\rangle$ as a function of the parameter ξ.

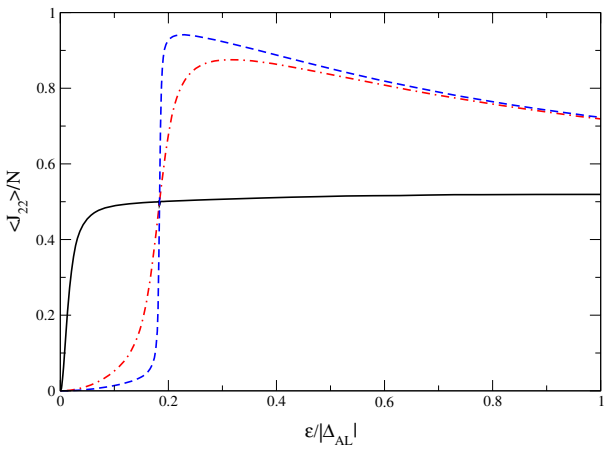

Figure 11. Atomic population per atom on the bare excited states $\langle J_{22}\rangle/N$ versus $\varepsilon/|\Delta|$ for $\gamma_-/\gamma_+ = 10^{-3}$, $\gamma_p/\gamma_+ = 0.5$, $\Delta = -1$, and for $N = 10$ (solid curve), 500 (dashed curve) and 5000 (dot-dashed curve).

The atomic population per atom on the upper bare state and the dressed state is given by [25]

$$\frac{\langle J_{22}\rangle}{N} = \left(1 - 2\sin^2\phi\right)\frac{\langle n\rangle}{N} + \sin^2\phi, \qquad \frac{\langle R_{22}\rangle}{N} = \frac{\langle n\rangle}{N}. \tag{4.17}$$

In the case when the number of atoms is very large, $N \gg 1$, this becomes

$$\frac{\langle R_{22}\rangle}{N} \cong \begin{cases} 1 & \text{if} \quad \xi > 1 \\ 1/2 & \text{if} \quad \xi = 1 \\ 0 & \text{if} \quad \xi < 1 \end{cases} \tag{4.18}$$

and

$$\frac{\langle J_{22}\rangle}{N} \cong \begin{cases} \cos^2\phi & \text{if} \quad \xi > 1 \\ 1/2 & \text{if} \quad \xi = 1 \\ \sin^2\phi & \text{if} \quad \xi < 1. \end{cases} \tag{4.19}$$

Clearly, the atomic population shows a sharp collective jump in which the active region of the photonic material switches from an absorptive medium to a gain medium as we change the intensity of the applied laser field (change in the control parameter, the angle ϕ). In this sense, the active region of the photonic material acts as an all-optical transistor, with a substantial optical differential gain for a relatively small change in the input intensity. Let us analyse the dependence of this jump on various parameters that enter its definition. For $N = 1$, the single-atom case, the atomic population per atom on the upper dressed state (in the Markovian model) is given by $\langle R_{22}\rangle/N = \xi/(\xi+1)$. Clearly, in the single-atom case, no sharp jump can be possible for this system configuration (smooth DOS over the spectral regions surrounding the Mollow spectrum components). The dephasing process has the tendency of diminishing the collective switching (by the dependence of ξ on γ_p). The unfavourable influence of the phonon-mediated dephasing on the collective switching can be reduced by increasing the atom number or by tuning the laser field frequency so that the coefficient of γ_p, $\sin^2\phi$, becomes very small. Clearly, the different mode densities experienced by the Mollow spectral components have a strong contribution in the collective switching of the atomic population. We present in figure 11 the dependence of $\langle J_{22}\rangle/N$ on the resonant

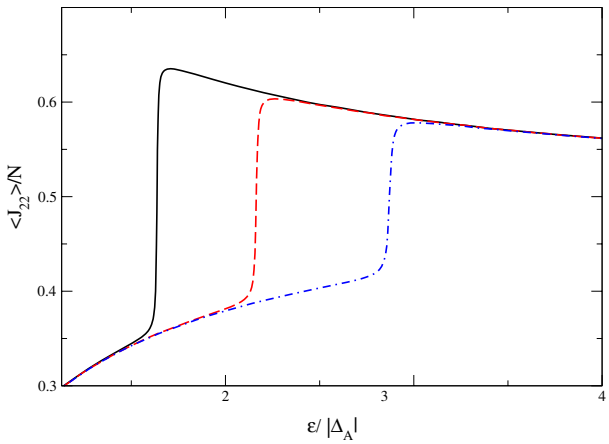

Figure 12. Atomic population per atom on the bare excited states $\langle J_{22}\rangle/N$ versus $\varepsilon/|\Delta_{AL}|$ for $\gamma_p/\gamma_+ = 0.5$, $\Delta_{AL} = -1$, $N = 5000$, and for $\gamma_-/\gamma_+ = 0.3$ (solid curve), $\gamma_-/\gamma_+ = 0.4$ (dashed curve), $\gamma_-/\gamma_+ = 0.5$ (dot-dashed curve).

Rabi frequency ε, in the case when we have considered a large jump in the photonic mode density of the confined photonic material, given by $\gamma_-/\gamma_+ = 10^{-3}$ and $\gamma_p/\gamma_+ = 0.5$.

Such a large jump may arise in a three-dimensional PBG material, but even if the jump is weaker (as for optical fibres [52] and optical wires [53]), a sizable switching behaviour is obtained for a sufficiently large number of atoms. For $\gamma_p/\gamma_+ = 0.5$ and $0.3 < \gamma_-/\gamma_+ < 0.5$, the collective switching behaviour is still important as shown in figure 12.

This switching behaviour characterizes the collective response of a large number of atoms (in previous plots $N = 5000$ for the most relevant case), and this collective response is possible when the left side-band lies near the gap of a PBG material or in the cut-off region of the optical fibres and wires, while the right side-band and the central component lie outside the gap or cut-off region. In the parametric conditions of figures 11 and 12, the system switches rapidly from the lower state to the upper state at a well defined critical value of the control parameter. We emphasize also that the collective timescale for this switching is proportional

to N^{-1}. Incorporation of non-Markovian effects near a three-dimensional photonic band edge leads to an even more dramatic collective timescale factor, which is proportional to N^{-2} [24]. This suggests that this effect may be relevant for very fast optical switching devices.

We introduce the Mandel q-parameter in order to characterize the atomic fluctuations in the excited bare and dressed states, defined by $Q_{\rm d} = (\langle R_{22}^2\rangle - \langle R_{22}\rangle^2)/\langle R_{22}\rangle$ and $Q_{\rm d} = (\langle J_{22}^2\rangle - \langle J_{22}\rangle^2)/\langle J_{22}\rangle$. In the limit of large number of atoms, the 'dressed' and 'bare' Mandel parameters become

$$Q_{\rm d} \cong \begin{cases} 1/N & \text{if} \quad \xi > 1 \\ N/12 & \text{if} \quad \xi = 1 \\ 1/(1-\xi) & \text{if} \quad \xi < 1, \end{cases} \tag{4.20}$$

$$Q_{\rm b} \cong \begin{cases} \sin^2\phi\,(1+\xi)/(1-\xi) & \text{if} \quad \xi > 1 \\ (N+2)/6 & \text{if} \quad \xi = 1 \\ \cos^2\phi\,(1+\xi)/(1-\xi) & \text{if} \quad \xi < 1. \end{cases} \tag{4.21}$$

Clearly, for $N \gg 1$ and $\xi > 1$, the q-Mandel parameter $Q_{\rm d} \cong 0$, i.e. the dressed-state atomic population inversion has a strong sub-Poissonian statistics. In contrast, the atomic statistics on the excited bare state $|2\rangle$ depends strongly on the dephasing rate $\gamma_{\rm p}$. If we assume that $\gamma_-/\gamma_+ \ll 1$, the q-Mandel parameter $Q_{\rm b}$ becomes $Q_{\rm b} \cong \cos^2\phi + 8\cos^2\phi\,\gamma_{\rm p}/\gamma_+$, which implies that $Q_{\rm b}$ goes to zero only if $\gamma_{\rm p}/\gamma_+ \ll 1$. In figure 13 we plot the q-Mandel parameter $Q_{\rm b}$ as a function of the resonance Rabi frequency ε, for the case of $N = 5000$ atoms, $\gamma_-/\gamma_+ = 10^{-3}$ and $0.5 < \gamma_{\rm p}/\gamma_+ < 0.01$, and an expanded view in the regime of sub-Poissonian statistics of the excited atoms, respectively. By analysing these figures, we note that at a critical value of the resonance Rabi frequency ε there is a strong (proportional to the number of atoms) increase in the atomic fluctuations, characteristic of a phase transition. For small dephasing rates as compared with the radiative decay rate outside the gap $\left(\gamma_{\rm p}/\gamma_+ = 0.01\right)$, the fluctuations in the excited state population, well above threshold, are very small. This may be relevant as a new mechanism of sub-Poissonian pumping for lasers [25].

5. Gain spectrum for a weak probe beam

In this section we analyse the gain spectrum of a second laser field which probes the driven atomic system. For simplicity of illustration, consider a single atom, driven by an external laser field, and placed in a photonic crystal, exhibiting a steplike discontinuity in the DOS (the one-atom version of the system analysed in the previous section). This simplified picture allows us to obtain analytical results and to provide a very intuitive picture of the switching and transistor action mechanisms in photonic crystals. It also provides a lower bound for the nonlinear switching effects. As discussed in the previous sections, there are two major enhancements to this worst case, the first coming from the non-Markovian character of a true band edge discontinuity (leading to lower threshold single-atom switching as presented in section 3), and the second one coming from the collective response of a system of two-level atoms placed in a photonic crystal (leading to larger differential gain and faster switching as presented in section 4). These additional effects provide a dramatic increase of the sensitivity, magnitude and speed of the switching and transistor effects.

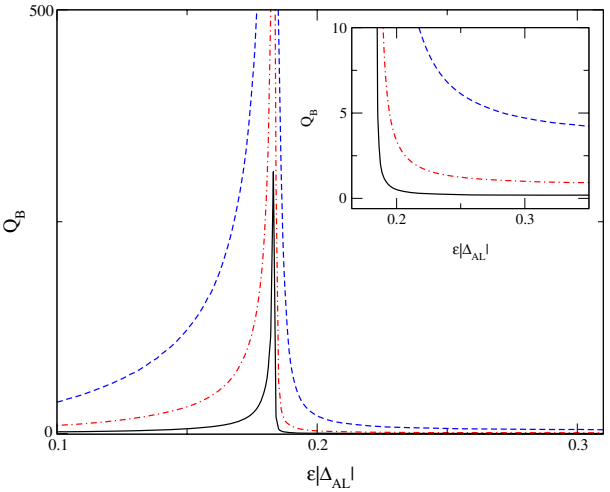

Figure 13. q-Mandel parameter $Q_{\rm b}$ as a function of $\varepsilon/|\Delta|$, $\gamma_-/\gamma_+ = 10^{-3}$, $\Delta = -1$, $N = 5000$, and for $\gamma_{\rm p}/\gamma_+ = 0.5$ (dashed curve), $\gamma_-/\gamma_+ = 0.1$ (dot-dashed curve) and $\gamma_-/\gamma_+ = 0.01$ (solid curve). The inset shows an expanded view of the same curves in the regime of sub-Poissonian statistics of excited atoms.

5.1. Dynamics and steady-state values of the atomic variables

In the case of a single atom ($N = 1$), the collective atomic operators J_{ij} of the previous section are replaced by their single-atom counterparts σ_{ij}, and the master equation is simplified by making use of the atomic operator products: $\sigma_{ij}\sigma_{kl} = \sigma_{jk}\delta_{il}$, $R_{ij}R_{kl} = R_{il}\delta_{jk}$, where $i, j, k, l = 1, 2$. For strong external laser fields or large detunings the master (4.8) can be solved exactly to yield

$$\langle R_\pm(t)\rangle = \langle R_\pm(0)\rangle e^{-\Gamma_\pm t}, \tag{5.1}$$

$$\langle R_3(t)\rangle = (\langle R_3(0)\rangle - \langle R_3\rangle_{\rm st})\, e^{-\Gamma_\pm t} + \langle R_3\rangle_{\rm st}, \tag{5.2}$$

where

$$\Gamma_0 = A_- + A_+, \qquad \Gamma_\pm = \frac{4A_0 + A_- + A_+}{2}, \qquad \langle R_3\rangle_{\rm st} = \frac{A_- - A_+}{A_- + A_+}, \tag{5.3}$$

and we use the notation $R_{21} = R_+$, $R_{12} = R_-$.

In order to understand steady-state positive atomic population inversion (shown in figures 14 and 15), we review the intuitive dressed atom picture. In the secular approximation, the dressed atom approach leads to a simple (although qualitative) interpretation of the dynamics of the atomic system and the characteristics of the scattered radiation [44, 54]. The bare (dressed) picture diagram is presented on the left (right) side of figure 16. We denote a state with the atom in its ith bare level and N photons in the background by the ket vector $|i, N\rangle$. The splitting between the states $|1, N+1\rangle$ and $|2, N\rangle$ is given by the detuning between the atomic and laser frequency $\Delta_{\rm AL} = \omega_{\rm A} - \omega_{\rm L}$. However, the states $|1, N+1\rangle$ and $|2, N\rangle$ are coupled by the laser mode–atom interaction Hamiltonian, the matrix element characterizing this interaction being proportional to the Rabi frequency ϵ: $\langle 2, N|H_{\rm AL}|1, N+1\rangle \approx \epsilon$. Since $\Delta_{\rm AL}$ and ϵ are small quantities compared with $\omega_{\rm L}$, we can neglect all the couplings between

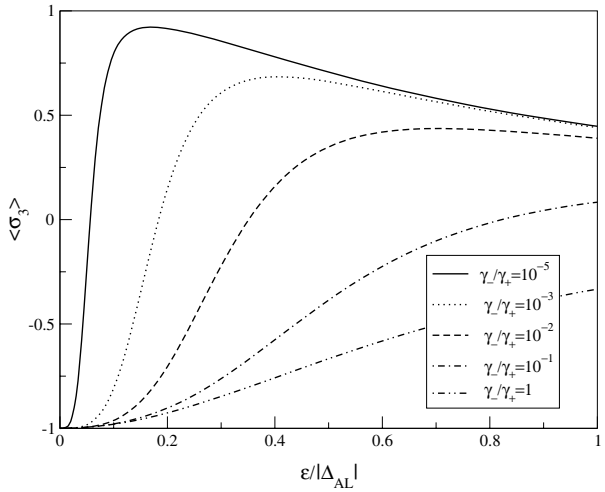

Figure 14. Steady-state atomic population inversion $\langle\sigma_3\rangle$ as a function of $\epsilon/|\Delta_{AL}|$ in the absence of the additional dephasing $\gamma_p = 0$. Different curves correspond to different ratios of the decay constants, varying from $\gamma_-/\gamma_+ = 10^{-5}$ (continuous curve) to $\gamma_-/\gamma_+ = 1$ (double-dot-dashed curve).

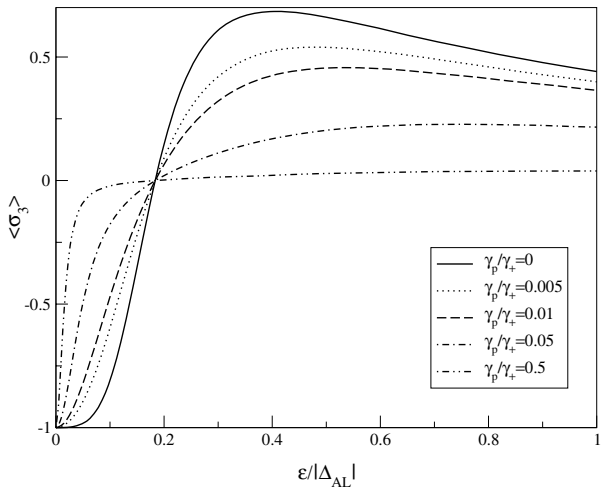

Figure 15. Steady-state atomic population inversion $\langle\sigma_3\rangle$ as a function of $\epsilon/|\Delta_{AL}|$ in the presence of the additional dephasing, and for $\gamma_p/\gamma_+ = 10^{-3}$. Different curves correspond to different ratios of the decay constants, varying from $\gamma_p/\gamma_+ = 0$ (continuous curve) to $\gamma_p/\gamma_+ = 0.5$ (double-dot-dashed curve).

different atom⊗laser manifolds, characterized by different numbers of photons in the laser field, N.

In the case of negative detunings of the atomic frequency with respect to the frequency of the laser field ($\mathrm{sign}(\Delta_{AL}) = 1$), we have $\sin(\phi) < \cos(\phi)$ and the dressed ground state, $|\tilde{1}\rangle$, is mostly comprised of the bare excited state $|2\rangle$, whereas the dressed excited state, $|\tilde{2}\rangle$, is mostly comprised of the bare ground state, $|1\rangle$. Also, from the dressed state diagram and the equation of evolution of the dressed state inversion (5.1), we note that the dressed excited state $|\tilde{2}\rangle$ is populated as a result of the transitions $|\tilde{1}\rangle \rightarrow |\tilde{2}\rangle$ (which occur at a rate $|\langle\tilde{1}, N|H_{int}|\tilde{2}, N-1\rangle|^2 = A_-$) and de-populated as a result of the transitions $|\tilde{2}\rangle \rightarrow |\tilde{1}\rangle$ (which occur at a rate $|\langle\tilde{2}, N|H_{int}|\tilde{1}, N-1\rangle|^2 = A_+$).

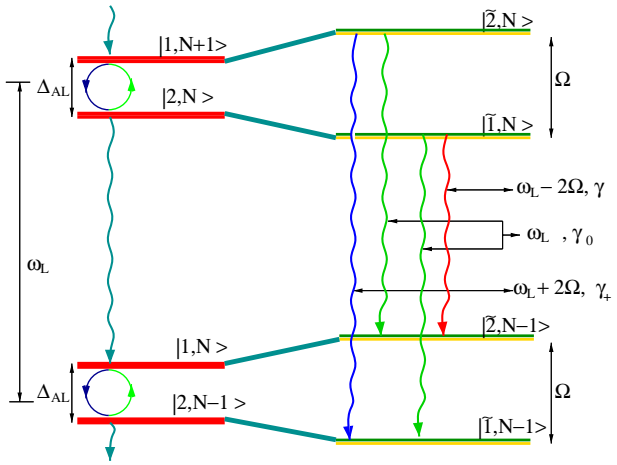

Figure 16. Bare atom and dressed atom state diagram.

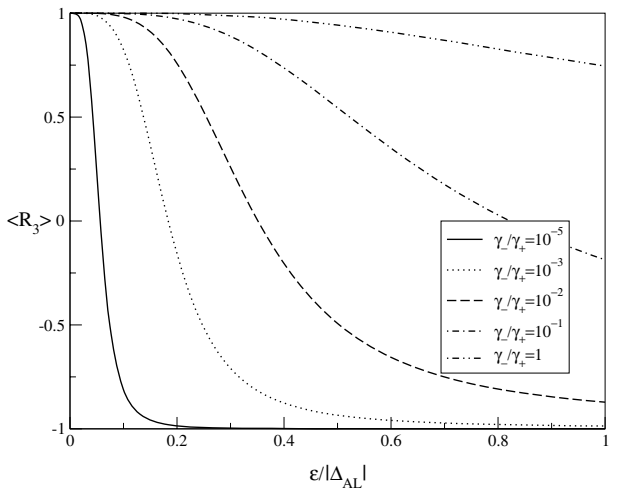

Figure 17. Dressed steady-state atomic population inversion $\langle R_3\rangle$ as a function of $\epsilon/|\Delta_{AL}|$ in the absence of the additional dephasing $\gamma_p = 0$. Different curves correspond to different ratios of the decay constants, varying from $\gamma_-/\gamma_+ = 10^{-5}$ (continuous curve) to $\gamma_-/\gamma_+ = 1$ (double-dot-dashed curve).

In the ordinary vacuum case ($\gamma_- = \gamma_+ = \gamma_0$), the rate of population of the dressed excited state $|\tilde{2}\rangle$ is always larger than the de-population rate (for $\Delta_{AL} < 0$, $\sin^2(\phi) > \cos^2(\phi) \Longrightarrow A_- > A_+$) and the dressed system will always end up in a stationary state with a larger population on the excited state $|\tilde{2}\rangle$ than the ground excited state $|\tilde{1}\rangle$. As the dressed excited state $|\tilde{2}\rangle$ is dominated by the bare ground state $|1\rangle$, the bare atomic system cannot be inverted [54]. In the case of a frequency-dependent reservoir ($\gamma_- \neq \gamma_0 \neq \gamma_+$), the inequality $A_- > A_+$ does not automatically hold. We can find a certain range for detunings, Δ_{AL} and Rabi frequencies, ϵ, such that, in the steady-state limit, the dressed state $|\tilde{2}\rangle$ is less populated than $|\tilde{1}\rangle$. The condition to preferentially populate the ground excited state $|\tilde{1}\rangle$ is

$$A_+ > A_- \quad \Longrightarrow \quad \gamma_+ c^4 > \gamma_- s^4. \tag{5.4}$$

We solve the threshold equation $A_+ = A_-$ to obtain the condition for switching. Using the dependence on $\sin(\phi)$ and $\cos(\phi)$ of the Rabi frequency ϵ, and introducing the new

variable $y = 1/\left(4\epsilon^2/\Delta_{\rm AL}^2 + 1\right)^{1/2}$ (subject to the constraint $0 \leqslant y \leqslant 1$), we obtain

$$\frac{\gamma_+ - \gamma_-}{4}\, y^2 - \frac{\gamma_+ + \gamma_-}{2}\, y + \frac{\gamma_+ - \gamma_-}{4} = 0. \tag{5.5}$$

If $\gamma_+ > \gamma_-$, (5.5) admits a single solution

$$y = \frac{\gamma_+ + \gamma_- - 2\sqrt{\gamma_+\,\gamma_-}}{\gamma_+ - \gamma_-}. \tag{5.6}$$

Or, equivalently, the threshold Rabi frequency can be expressed as

$$\frac{\epsilon_{\rm thr}}{|\Delta_{\rm AL}|} = \frac{\sqrt[4]{\gamma_+\gamma_-}}{\sqrt{\gamma_+} - \sqrt{\gamma_-}} = \sqrt[4]{\frac{\gamma_-}{\gamma_+}} \times \left[1 - \sqrt{\frac{\gamma_-}{\gamma_+}}\right]. \tag{5.7}$$

We note the threshold Rabi frequency depends only on the detuning and the relative magnitude of the jump in the photonic DOS (through the ratio γ_-/γ_+). The decay constant γ_0, and the dephasing rate $\gamma_{\rm p}$ do not affect the threshold intensity since their effect is to populate and depopulate the dressed states $|\tilde{1}\rangle$, $|\tilde{2}\rangle$ at the same rate.

In figure 17 we plot the 'dressed' steady-state atomic population inversion R_3, as a function of the resonance Rabi frequency for different magnitudes of the jump in the photonic DOS, γ_-/γ_+.

5.2. Absorption and dispersion of a weak probe beam

We now consider that in addition to the pump laser field, the atomic system is probed by a second laser field, of frequency ω [55–57]. The probe field is assumed to be sufficiently weak to not disturb the dressed picture of the atomic system. The linear susceptibility of this system is given in terms of an electric field correlation function evaluated in the absence of the probe field [44]

$$\chi(\omega) = {\rm i}\mathcal{A}\int_0^\infty \langle[\mathcal{E}_+(t),\, \mathcal{E}_-]\rangle_{\rm st} {\rm e}^{{\rm i}\omega t}\, {\rm d}t. \tag{5.8}$$

Here $\mathcal{A}$ is a normalization constant, the index s indicates that the average is evaluated in the steady-state limit and $\mathcal{E}_\pm$ are the positive and negative frequency components of the scattered electric field. In the ordinary vacuum case ($\gamma_- = \gamma_+ = \gamma_0$), the positive and negative frequency components of the scattered electric field are taken to be proportional to the atomic dipole operator

$$\sigma_{12}(t) = cs R_3 {\rm e}^{-{\rm i}\omega_{\rm L} t} - s^2 R_{12} {\rm e}^{-{\rm i}(\omega_{\rm L} - 2\Omega)t} + c^2 R_{21} {\rm e}^{-{\rm i}(\omega_{\rm L} + 2\Omega)t}. \tag{5.9}$$

However, in the case of a photonic crystal, the atomic-dipole moment has spectral components that encounter different photonic DOSs, and, implicitly, have different radiative rates (γ_0, γ_-, γ_+). In equation (3.10*a*), which describes the temporal evolution of the λ-mode annihilation operator, a_λ, there is a clear correlation between the frequency at which the 'source operators' R_3, R_{12} and R_{21} oscillate (Δ_λ, $\Delta_\lambda \pm 2\Omega$, respectively) and the photonic DOS available for the specific λ-mode considered (through the λ dependence of the coupling constant g_λ). Accordingly, the positive and negative frequency components of the scattered electric field are given by [58]

$$\mathcal{E}^+(t) = \sqrt{\frac{\gamma_0}{2}}\, cs R_3(t) + \sqrt{\frac{\gamma_+}{2}}\, c^2 R_{12}(t) {\rm e}^{-2{\rm i}\Omega t} - \sqrt{\frac{\gamma_+}{2}}\, s^2 R_{21}(t) {\rm e}^{2{\rm i}\Omega t}, \tag{5.10}$$

$$\mathcal{E}^-(t) = \left[\mathcal{E}^-(t)\right]^\dagger. \tag{5.11}$$

Using (5.10) and the fact the off-diagonal elements of the density matrix operator vanish in the stationary limit, in the strong-driving-field limit the central component at the frequency $\omega_{\rm L}$ disappears, and the linear susceptibility has two well separated components, at the frequencies $\omega_{\rm L} \pm 2\Omega$ [44,54]

$$\chi(\omega) = \chi^{(+)}(\omega) + \chi^{(-)}(\omega), \tag{5.12}$$

with

$$\chi^{(+)}(\omega) = {\rm i}\mathcal{A}\gamma_+ c^4 \int_0^\infty \langle[R_{12}(t),\, R_{21}]\rangle_{\rm st} {\rm e}^{{\rm i}[\omega - (\omega_{\rm L} + 2\Omega)]t}\, {\rm d}t, \tag{5.13}$$

$$\chi^{(-)}(\omega) = {\rm i}\mathcal{A}\gamma_- s^4 \int_0^\infty \langle[R_{21}(t),\, R_{12}]_s\rangle {\rm e}^{{\rm i}[\omega - (\omega_{\rm L} - 2\Omega)]t}\, {\rm d}t. \tag{5.14}$$

The correlation function present in (5.13) can be evaluated using the quantum regression theorem [59]

$$[R_{21}(t),\, R_{12}] = [R_{21},\, R_{12}]\ {\rm e}^{-\Gamma_\pm t} \tag{5.15}$$

$$[R_{12}(t),\, R_{21}] = [R_{12},\, R_{21}]\ {\rm e}^{-\Gamma_\pm t} \tag{5.16}$$

where $\Gamma_\pm$ are defined in (5.3). Finally, the real and imaginary parts of components of the linear susceptibility $\chi(\omega)$ in the Markovian approximation are given by

$$\chi_R^{(+)}(\omega) = \mathcal{A}\,\gamma_+\, c^4\,(P_+ - P_-) \cdot \frac{\omega - (\omega_{\rm L} + 2\Omega)}{[\omega - (\omega_{\rm L} + 2\Omega)]^2 + \Gamma_\pm^2}, \tag{5.17}$$

$$\chi_R^{(-)}(\omega) = \mathcal{A}\,\gamma_-\, s^4\,(P_- - P_+) \cdot \frac{\omega - (\omega_{\rm L} - 2\Omega)}{[\omega - (\omega_{\rm L} - 2\Omega)]^2 + \Gamma_\pm^2}, \tag{5.18}$$

$$\chi_I^{(+)}(\omega) = -\mathcal{A}\,\gamma_+\, c^4\,(P_+ - P_-) \cdot \frac{\Gamma_\pm}{[\omega - (\omega_{\rm L} + 2\Omega)]^2 + \Gamma_\pm^2}, \tag{5.19}$$

$$\chi_I^{(-)}(\omega) = -\mathcal{A}\,\gamma_-\, s^4\,(P_- - P_+) \cdot \frac{\Gamma_\pm}{[\omega - (\omega_{\rm L} - 2\Omega)]^2 + \Gamma_\pm^2} \tag{5.20}$$

where $P_\pm$ represent the dressed excited and ground state populations given by

$$P_+ = \langle R_{22}\rangle_{\rm st} = \frac{A_-}{A_- + A_+} \tag{5.21}$$

$$P_- = \langle R_{11}\rangle_{\rm st} = \frac{A_+}{A_- + A_+}. \tag{5.22}$$

Similar to the ordinary vacuum case [55], the imaginary part of the linear susceptibility consists in one absorptive component and one amplifying component (note the sign difference between $\chi_I^{(+)}$ and $\chi_I^{(+)}$). In contrast to ordinary vacuum, the photonic crystal allows us to control the absorptive or amplifying character of the individual components (through variations in the intensity of the driving laser field).

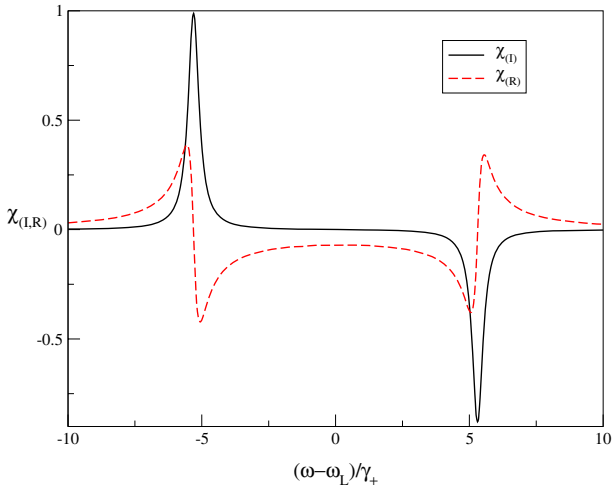

Figure 18. The real and imaginary parts of the linear susceptibility of the probe beam as a function of the detuning of the probe beam frequency, ω, with respect to the driving laser field frequency $\omega_{\rm L}$, for $\epsilon/|\Delta_{\rm AL}| = 0.178$, $\gamma_-/\gamma_+ = 0.001$, $\gamma_0/\gamma_+ = 1$, $\epsilon/\gamma_+ = 2.5$ and in the presence of a small amount of phonon-mediated dephasing, $\gamma_{\rm p}/\gamma_+ = 0.1$. The atomic resonant frequency is detuned negatively from the laser field frequency, $\Delta_{\rm AL} = \omega_{\rm A} - \omega_{\rm L} < 0$.

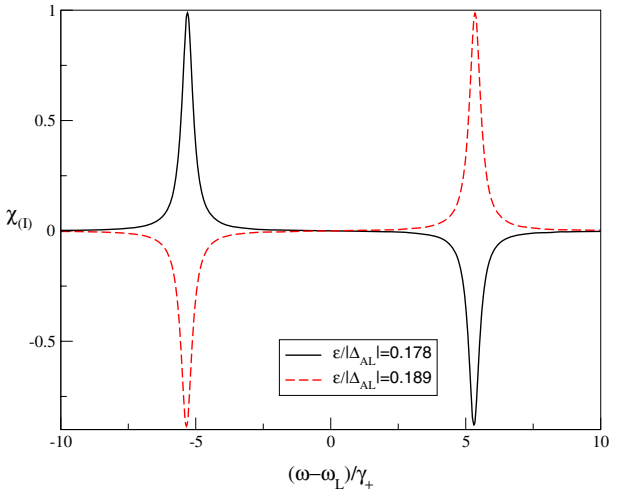

Figure 19. The imaginary part of the linear susceptibility of the probe beam (absorption spectrum) as a function of the detuning of the probe beam frequency, ω, with respect to the driving laser field frequency $\omega_{\rm L}$, for $\gamma_-/\gamma_+ = 0.001$, $\gamma_0/\gamma_+ = 1$, $\epsilon/\gamma_+ = 2.5$ and in the presence of a small amount of phonon-mediated dephasing, $\gamma_{\rm p}/\gamma_+ = 0.1$. The two curves correspond to different Rabi frequencies, $\epsilon/|\Delta_{\rm AL}|$, one of them (continuous curve) below the inversion threshold $\epsilon/|\Delta_{\rm AL}| = 0.178$, and the other one (dashed curve) above the threshold intensity $\epsilon/|\Delta_{\rm AL}| = 0.189$. The atomic resonant frequency is detuned negatively from the laser field frequency, $\Delta_{\rm AL} = \omega_{\rm A} - \omega_{\rm L} < 0$, and for this choice of parameters, the threshold intensity is $\epsilon_{\rm thr}/|\Delta_{\rm AL}| = 0.183$.

In particular, it is possible to switch a given sideband from being absorptive to exhibiting gain through a small change in the pump laser intensity. This property can be easily understood using the dressed-state diagram depicted in figure 16. Unlike the fluorescence spectrum, the absorption signal is proportional to the difference of the population between the dressed levels involved in the transition (multiplied by the transition rate between the levels). In contrast, the fluorescent signal depends only on the population of the initial state of the transition (multiplied by the transition rate) [44, 54]. Clearly, the character of the absorption signal components is determined by the sign of the dressed atomic inversion, which in turn is determined by the intensity of the driving field (see figure 19). In figure 18, we plot the real and imaginary parts of the linear susceptibility of the probe beam as a function of the detuning of the probe beam frequency, ω, with respect to the driving laser field frequency $\omega_{\rm L}$, for $\epsilon/|\Delta_{\rm AL}| = 0.178$, $\gamma_-/\gamma_+ = 0.001$, $\gamma_0/\gamma_+ = 1$, $\epsilon/\gamma_+ = 2.5$ and in the presence of a small amount of phonon-mediated dephasing, $\gamma_{\rm p}/\gamma_+ = 0.1$.

In ordinary vacuum, one Mollow sideband exhibits weak gain and the other sideband exhibits strong absorption. However, there is no switching of a given sideband with pump intensity. In the photonic crystal switching takes place. Moreover, the amplitude of the amplifying component is of the same order of magnitude as the amplitude of the absorbing component and easily detectable in a pump–probe spectroscopy experiment. The components are separated by a spectral distance proportional to the intensity of the driving field and their relative magnitude can be optimized by variations in the driving field. In figure 20, we show the gradual transition through the threshold region of the imaginary part of the susceptibility of the probe beam and note that the threshold point (in the $\epsilon/|\Delta_{\rm AL}|$ parameter space) is characterized by a total transparency of the active medium. As the intensity of the driving laser field passes through the threshold intensity,

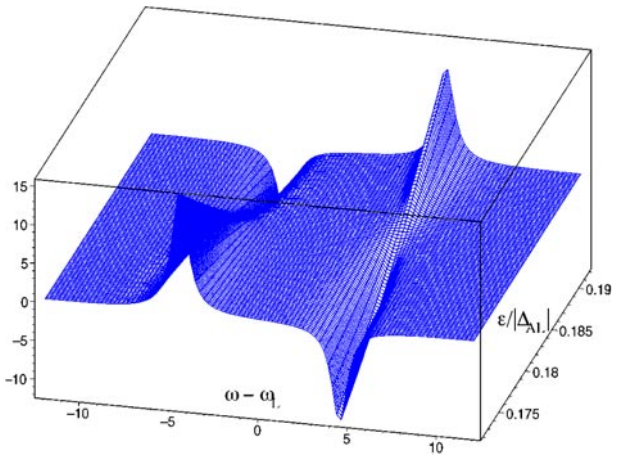

Figure 20. The imaginary part of the linear susceptibility of the probe beam as a function of the detuning of the probe beam frequency, ω, with respect to the driving laser field frequency $\omega_{\rm L}$, and the Rabi frequency of the driving laser field $\epsilon/|\Delta_{\rm AL}|$, for $\gamma_-/\gamma_+ = 0.001$, $\gamma_0/\gamma_+ = 1$, and in the absence of the phonon-mediated dephasing, $\gamma_{\rm p} = 0$. The atomic resonant frequency is detuned negatively from the laser field frequency, $\Delta_{\rm AL} = \omega_{\rm A} - \omega_{\rm L} < 0$.

the active medium switches from an absorptive medium to a gain medium at a relatively well defined intensity of the driving field.

6. Conclusions

We have analysed the atomic switching in photonic crystals using two simple models and suggested its relevance to all-optical transistor action. As a function of the intensity of the

pump (control) laser, the active region of a photonic material (the atomic system) sharply switches from an absorptive medium (the atom spends most of its time in the ground state) to a gain medium (higher probability to find the atom in its excited state). This is a very fundamental effect arising from the modification of the electromagnetic vacuum in a photonic crystal. This effect is forbidden in ordinary vacuum by the Einstein rate equations. We have shown that a weak second probe laser beam experiences a substantial differential gain when the pump (control) laser intensity is in the neighbourhood of the threshold value. This switching of the response of a probe beam (at a given frequency) to a small change in the pump (control) beam is absent in ordinary vacuum. In the first model, we considered an atom in a PBG material coupled to a three-dimensional photonic band edge and driven by an external laser field of moderate intensity. Using a non-Markovian analysis of the system, we demonstrated switching behaviour as a function of both laser field intensity and detuning frequency. The condition that triggers this jump in the atomic population inversion corresponds to driving the left component of the atomic spectrum inside the gap, while the central resonance and the right side band remain outside the gap. In the second model, we presented an analysis of the population inversion and the excitation statistics of two-level atoms, driven by a strong laser field, in a vacuum with a step discontinuity in the electromagnetic DOS. Assuming a moderately strong pump laser, we used a Markov approximation for radiative dynamics and demonstrated collective switching and sub-Poissonian atomic population statistics. For a large number of atoms, even when the discontinuity in the photonic DOS is not so large, the switching occurs, albeit at a higher pump threshold.

Based on these two simple models we suggest that if *both* non-Markovian and collective enhancement are incorporated in a single model, many desirable features of all-optical switching and all-optical transistor action will follow. These include low pumping threshold, very large differential optical gain and very fast response time, all in a very compact (20 μm scale) device. In addition to steady-state operation as an all-optical transistor, it is of considerable interest to modulate the pump (control) field with input from an optical communication network. In this case, picosecond pulses of light could modulate the total pump (control) field back and forth across the switching threshold. In this way, pulses of light from the probe beam could be routed (amplified rather than absorbed) through the device, depending on whether a pulse from the pump field has reached the device. This provides an all-optical packet switching function. Since the gain spectrum experienced by the probe beam can be controllably displaced in frequency from the (modulated) pump frequency, this system could be used as an all-optical wavelength converter for data, from the pump to the probe. The relatively narrow spectral range of amplification of the proposed device can be dramatically increased by using an inhomogeneous active medium, with a broad distribution of resonant atomic transition frequencies. This occurs quite naturally if the active layers consist of quantum dots exhibiting a distribution of sizes. In this case the gain spectrum (and corresponding bandwidth of the switching device) may be considerably broadened relative to the narrow fluorescence side band shown in figure 19. A second type of inhomogenous broadening occurs due to local environments experienced by individual quantum dots. In particular, the local electromagnetic DOS will vary from point to point in space, leading to broadening of the spectral region available for switching. It is of considerable interest in this context to evaluate local density of states (LDOS) discontinuities for realistic device heterostructures and to examine in detail the relationship between the switching threshold energies, switching speeds and corresponding coupling speeds of optical information in and out of the device.

A physical realization of this all-optical switching system could come from the growth of a III–IV semiconductor device heterostructure around a suitable PBG template. The heterostructure would consist of an active region of quantum dots sandwiched within a planar waveguide with an engineered electromagnetic DOS, between semiconductor cladding layers above and below exhibiting a large three-dimensional PBG. The quantum dots would then 'feel' the electromagnetic DOS presented by the defect layer within the larger PBG. Due to the size distribution of quantum dots, there would be a natural broadening of the gain spectrum experienced by the probe beam as discussed above. Positional randomness of the dots within the semiconductor backbone would also lead to 'inhomogeneous' broadening of the switching threshold. An alternative realization of the effects described in this paper is through trapping and cooling real atoms in the void regions of a PBG crystal. The electric field distribution for a laser mode in the vicinity of the upper band edge (the so called 'air' band) has strong intensity peaks in the void region of the material, which can act as an optical trap for active atoms [43, 60]. The trapped atoms will exhibit little interaction with the lattice of the dielectric host, thus minimizing additional decay and dephasing effect. A third possible realization of the all-optical switching we discussed, is from real atoms embedded in the dielectric backbone of a PBG material. The radiative transition of the erbium atom comes from the atomic 4f shell, which is screened by the outer shells from the environmental influence. At low temperatures, the erbium atoms suitably implanted in a silicon-based PBG material may have very sharp single-atom-like features [61] (the most intense line at 1.537 μm has a full width of 0.0005 μm).

Clearly, the experimental observation of atomic switching depends strongly on the influence of the dielectric host material on the active atoms. By including these effects in our calculations, we have shown that a sizable switching effect is present even in the presence of nonradiative decay and dephasing contribution ($0.08\gamma \leqslant 1/T_1^{\rm nr}, 1/T_2 \leqslant \gamma$). The influence of dephasing is weaker than that of the nonradiative decay. In our model involving a single atom near a three-dimensional photonic band edge, switching occurs when $\Omega \approx \beta_{\rm A}$, where Ω is the generalized Rabi frequency, and $\beta_{\rm A}$ is the typical timescale of the atomic system evolution. Since $\beta_{\rm A}$ depends strongly on the specific photonic crystal used, we limit ourselves to general considerations about the order of magnitude of the laser field intensity, I, required to produce switching. If we neglect the detuning of the atomic frequency with respect to the laser frequency, it can be easily shown that [62]

$$\left|\frac{\Omega}{2\pi}\,[\mathrm{Hz}]\right| = \frac{|\boldsymbol{d}_{21}\cdot\boldsymbol{e}_{\mathrm{L}}|}{ea_0}\sqrt{\frac{2e^2a_0^2}{\varepsilon_0\hbar^2c}}\sqrt{I\left[\mathrm{W\ m^{-2}}\right]}$$
$$= 0.22\times10^7\frac{|\boldsymbol{d}_{21}\cdot\boldsymbol{e}|}{ea_0}\sqrt{I\left[\mathrm{W\ m^{-2}}\right]}. \qquad (6.1)$$

For a typical optical transition (with dipole moments between 10^{-1} and 10^1 au) a laser field of 0.5 mW mm^{-2} intensity will produce a Rabi frequency of 0.1 GHz (which is of the order of magnitude of β_{A}). Including non-Markovian dynamics and collective effects of many atoms within a single model should improve this estimate considerably.

The central question in the realization of a PBG all-optical transistor is whether dielectric microstructure exhibiting a sufficiently large jump in the local electromagnetic DOS over a sufficiently small frequency interval can be realized in practice. While an ideal band edge exhibits a large jump, it is well known that the DOS associated with a real band edge can differ considerably from that of mathematical idealization when disorder effects and finite sample effects are considered. Another option is to engineer a more specific DOS profile by selectively introducing defect bands inside the large three-dimensional PBG of the host photonic crystal. This may offer more flexibility in designing the optimum device heterostructure.

References

[1] Gibbs H M 1985 *Optical Bistability: Controlling Light with Light* (New York: Academic)
[2] Miller D A B 1989 *Optical Computing: Proc. 34th Scottish Universities Summer School in Physics (Edinburgh, 1988)* ed B S Wherrett and F A P Tooley (Bristol: Hilger)
[3] Gibbs H M *et al* 1976 *Phys. Rev. Lett.* **36** 1135
[4] Protsenko I E and Lugiato L A 1994 *Phys. Rev.* A **50** 1627
[5] Protsenko I E and Lugiato L A 1991 *Opt. Commun.* **109** 304
[6] McCall S L *et al* 1975 *Bull. Am. Phys. Soc.* **20** 636
[7] Miller D A B and Smith S D 1979 *Opt. Commun.* **31** 101
[8] Tooley F A P, Smith S D and Seaton C T 1983 *Appl. Phys. Lett.* **43** 807
[9] DeSalve *et al* 1992 *Opt. Lett.* **17** 28
[10] Stegeman G I *et al* 1993 *Opt. Lett.* **18** 13
[11] Kim S *et al* 1998 *IEEE J. Quantum Electron.* **34** 666
[12] Assanto G *et al* 1993 *Appl. Phys. Lett.* **62** 1323
[13] Schiek R 1993 *J. Opt. Soc. Am.* **10** 1848
[14] Assanto G *et al* 1995 *IEEE J. Quantum Electron.* **31** 673
[15] Saltiel S, Buchvarov I and Koynov K 1999 *Advanced Photonics with Second-Order Nonlinear Processes* ed A Boardman (Dordrecht: Kluwer)
[16] Russell P St 1993 *Electron. Lett.* **29** 1228
[17] Russell P St 1991 *IEEE J. Quantum Electron.* **27** 830
[18] Fujimura M, Suhara T and Nishihara H 1992 *Electron. Lett.* **28** 721
[19] Coriasso C *et al* 1998 *Opt. Express* **3** 454
[20] Yoffe G W *et al* 1993 *Appl. Phys. Lett.* **63** 2318
[21] John S 1984 *Phys. Rev. Lett.* **53** 2169
[22] John S 1987 *Phys. Rev. Lett.* **58** 2486
[23] Yablonovitch E 1987 *Phys. Rev. Lett.* **58** 2059
[24] John S and Quang T 1994 *Phys. Rev.* A **50** 1764
Kaufman A, Kurizki G and Sherman B 1994 *J. Mod. Opt.* **41** 353
Lewenstein M, Zakrzewski J and Mossberg T W 1988 *Phys. Rev.* A **38** 808
Yang Y and Zhu S Y 2000 *Phys. Rev.* A **62** 013805
[25] John S and Quang T 1997 *Phys. Rev. Lett.* **78** 1888
[26] Vats N and John S *Phys. Rev.* A **58** 4168
[27] John S and Quang T *Phys. Rev.* A **54** 4479
[28] Loudon R 1995 *The Quantum Theory of Light* (Oxford: Oxford University Press)
[29] Florescu M and John S 2001 *Phys. Rev.* A **64** 033801
[30] Weinrech G 1965 *Solids* (New York: Wiley)
[31] Yablonovitch E, Gmitter T J and Leung K M 1991 *Phys. Rev. Lett.* **67** 2295
[32] Lin S Y *et al* 1998 *Nature* **394** 251
[33] Ho K M *et al* 1993 *Solid State Commun.* **89** 413
[34] Birner A *et al* 2001 *Adv. Mater.* **13** 377
[35] Cristophersen M *et al* 2000 *Mater. Sci. Eng.* B **69** 194
[36] Klose R and Dichtel K unpublished
[37] Wos W L 1996 *Phys. Rev.* B **53** 16 231
[38] Winjnhoven J E G L and Vos W L 1998 *Science* **281** 802
[39] Miguez H *et al* 1999 *Phys. Rev.* B **59** 1563
[40] Vlasov Y A, Yao N and Norris D J 1999 *Adv. Mater.* **11** 165
[41] Blanco A *et al* 2000 *Nature* **405** 437
[42] Toader O and John S 2001 *Science* **229** 5519
[43] Toader O, John S and Busch K 2001 *Opt. Express* **8** 272
[44] Cohen-Tannoudji C, Dupont-Roc J and Grynberg 1992 *Atom–Photon Interactions* (New York: Wiley-Interscience)
Mollow B R 1972 *Phys. Rev.* A **5** 2217
Freedhoff H and Quang T 1994 *J. Opt. Soc. Am.* B **12** 474
[45] Murli A and Rizzardi M 1990 *ASSOC. for Comput. Machinery, Transactions on Math. Software* **16** 158
Cheng A H, Sidauruk P and Abousleiman Y 1994 *Math. J.* **4** 56
[46] Narducci L M *et al* 1978 *Phys. Rev.* A **18** 1971
[47] Machida S, Yamamoto Y and Itaya Y 1987 *Phys. Rev. Lett.* **58** 100
[48] Golubev Y M and Sokolov I V 1984 *Zh. Eksp. Teor. Fiz.* **87** 408
Golubev Y M and Sokolov I V 1984 *Sov. Phys.–JETP* **60** 234
Marte M A M and Zoller P 1989 *Phys. Rev.* A **40** 5774
Bergou J *et al* 1989 *Phys. Rev.* A **40** 5073
[49] Carmichael H 1993 *An Open Systems Approach to Quantum Optics* (Berlin: Springer)
[50] Quang Tran 1991 *Phys. Rev.* A **43** 2561
Bogolubov N N Jr, Shumovsky A S and Quang Tran 1987 *Opt. Commun.* **64**
[51] Kowalewska-Kudłaszyk A, Tanaś R and Tanas R 2000 *Acta Phys. Slov.* **50** 313
[52] Kleppner D 1981 *Phys. Rev. Lett.* **47** 233
[53] Brorson S D, Yokoyoma H and Ippen E P 1990 *IEEE J. Quantum Electron.* **26** 1492
[54] Cohen-Tannoudji C and Reynaud S 1978 Multiphoton processes *Proc. Int. Conf. (Rochester, 1977)* ed J H Eberly and P Lambropoulos (New York: Wiley)
[55] Mollow B R 1972 *Phys. Rev.* A **5** 2217
[56] Erhard E and Keitel C H 2000 *Opt. Commun.* **179** 517
[57] Kocharovskaya O and Radeonychev Y Y 1996 *Quantum Semiclass. Opt.* **7** 17
[58] Mosseberg T W and Lewenstein M 1993 *J. Opt. Soc. Am.* B **10** 340
[59] Lax M 1968 *Phys. Rev.* **172** 350
[60] Woldeyohannes M and John S 1999 *Phys. Rev.* A **60** 5046
[61] Lanzerstorter S *et al* 1998 *Appl. Phys. Lett.* **72** 809
Masterov V F *et al* 1998 *Appl. Phys. Lett.* **72** 728
Komuro S *et al* 1999 *Appl. Phys. Lett.* **74** 377
[62] Shore B W *The Theory of Coherent Atomic Excitation* (New York: Wiley)